

# REPORT No. 833

## GENERAL THEORY OF AIRFOIL SECTIONS HAVING ARBITRARY SHAPE OR PRESSURE DISTRIBUTION

By H. JULIAN ALLEN

### SUMMARY

*In this report a theory of thin airfoils of small camber is developed which permits either the velocity distribution corresponding to a given airfoil shape, or the airfoil shape corresponding to a given velocity distribution to be calculated. The procedures to be employed in these calculations are outlined and illustrated with suitable examples.*

### INTRODUCTION

Before the advent of the low-drag and high-critical-speed airfoils, the shapes of airfoil sections having desirable aerodynamic characteristics were found by the purely empirical method of testing families of related profiles. The pressure distribution over any of these shapes could be calculated by any of a number of methods, but notably by the method of references 1 and 2.

Subsequently, experimental and theoretical investigations, on the one hand, of the laminar boundary layer and the phenomenon of transition and, on the other, of the compression shock wave promoted a better understanding of the factors affecting the drag of airfoils. It became apparent that the control of the aerodynamic characteristics of airfoils was to be found in the control of the pressure or velocity distribution. Hence, in the design of an airfoil having certain desirable aerodynamic characteristics, the "inverse" problem of finding the shape of an airfoil which would promote a specified velocity distribution over its surface became of considerable importance.

One notable method has been advanced (reference 3) for solving this inverse problem. However, this method is intricate and laborious to employ.

In this report a new method, which has been used for the past several years in the design of a large number of low-drag and high-critical-compressibility-speed airfoils, is presented. This method, which is comparatively rapid and easily applied, may be used to solve either the direct or the more important inverse problem. Illustrative examples are included.

### THEORY

It is shown in reference 4 that in a determination of the pressure distribution over a cambered airfoil the effects of the camber and the thickness distribution may be considered independently. Specifically, it is shown that the induced velocity at any point on the cambered airfoil may be found

by superposing the induced velocity at the point due to the vortex system, which may be considered to replace the mean camber line, and that at the point due to the source-sink system, which may be considered to replace the "base profile." The base profile of the airfoil is the profile if the camber were removed and the resulting symmetrical airfoil set at zero angle of attack. In the airfoil theory of this report it is convenient to consider separately the base profile and the mean camber line which together make up a given airfoil.

### CAMBER-LINE THEORY

Glauert (reference 5) has considered the problem of the mean camber line which, in a more convenient form for calculation and extended so as to include the theory of the strut as well as airfoil mean camber lines, is given in the following:

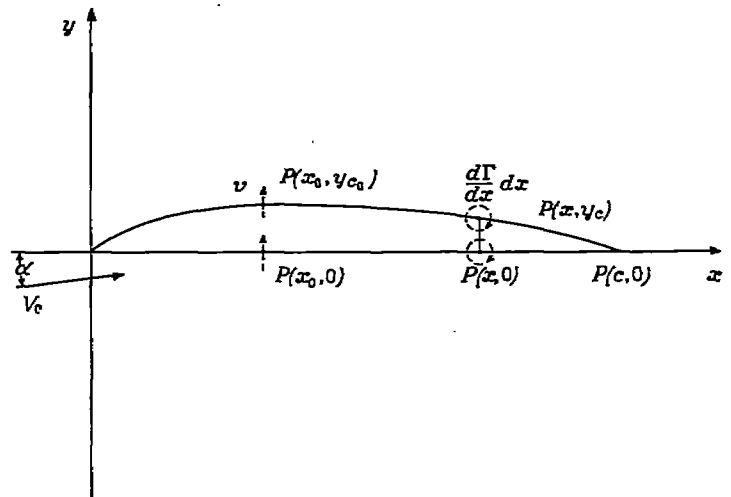


FIGURE 1.—Diagram of mean camber line.

Consider the mean camber line shown in figure 1. If the camber is small, the velocity induced at a point  $P(x_0, y_c)$  on the mean camber line by a vortex at any other point  $P(x, y_c)$  on this line is approximately that which would be induced at the point on the x-axis  $P(x_0, 0)$  by the same vortex at the point  $P(x, 0)$ . If the vortex strength at any point is  $\frac{d\Gamma}{dx} dx$ , the velocity induced at any point on the camber line due to all the vortices distributed along the camber line is

$$v(x_0) = \frac{1}{2\pi} \int_0^c \frac{\frac{d\Gamma}{dx} dx}{(x-x_0)} \quad (1)$$

and is perpendicular to the  $x$ -axis. The flow direction close to the camber line must be parallel to the surface of the camber line so that if the angle  $\alpha$  between the  $x$ -axis and the flow direction of the undisturbed stream is small, then

$$\frac{v}{V_0} = \frac{dy_c}{dx} - \alpha \quad (2)$$

where  $V_0$  is the velocity of the undisturbed stream.

It is convenient to introduce the new coordinate  $\theta$  for  $x$  such that

$$\left. \begin{aligned} x &= \frac{c}{2} (1 - \cos \theta) \\ x_0 &= \frac{c}{2} (1 - \cos \theta_0) \\ dx &= \frac{c}{2} \sin \theta d\theta \end{aligned} \right\} \quad (3)$$

where  $c$  is the airfoil chord. Assuming the distribution of vorticity  ${}_0\Gamma$  (where the prescript  ${}_0$  indicates that this circulation applies to an airfoil of zero thickness) along the  $x$ -axis is

$$\frac{d{}_0\Gamma}{dx} = 2V_0 \left( A_0' \cot \frac{1}{2} \theta + A_0'' \tan \frac{1}{2} \theta + \sum_1^{\infty} A_n \sin n\theta \right) \quad (4)$$

Then

$$\begin{aligned} \frac{d{}_0\Gamma}{dx} dx &= cV_0 \left[ A_0' (1 + \cos \theta) + A_0'' (1 - \cos \theta) \right. \\ &\quad \left. + \sum_1^{\infty} A_n \sin n\theta \sin \theta \right] d\theta \end{aligned} \quad (5)$$

Writing  $\sin n\theta \sin \theta = \frac{1}{2} [\cos (n-1)\theta - \cos (n+1)\theta]$ , then from equations (1), (2), (3), and (5) the slope at  $\theta_0$  may be obtained from

$$\begin{aligned} \frac{dy_{c_0}}{dx} - \alpha &= \frac{1}{\pi} \int_0^{\pi} \left\{ \frac{A_0' (1 + \cos \theta) + A_0'' (1 - \cos \theta)}{\cos \theta_0 - \cos \theta} \right. \\ &\quad \left. + \frac{\frac{1}{2} \sum_1^{\infty} A_n [\cos (n-1)\theta - \cos (n+1)\theta]}{\cos \theta_0 - \cos \theta} \right\} d\theta \end{aligned} \quad (6)$$

It is shown in reference 5 that

$$\int_0^{\pi} \frac{\cos n\theta}{\cos \theta - \cos \theta_0} d\theta = \pi \frac{\sin n\theta_0}{\sin \theta_0} \quad (7)$$

so that equation (6) becomes for the slope at  $\theta$

$$\frac{dy_c}{dx} = \alpha - A_0' + A_0'' + \sum_1^{\infty} A_n \cos n\theta \quad (8)$$

The coefficients are given by

$$\left. \begin{aligned} \alpha - A_0' + A_0'' &= \frac{1}{\pi} \int_0^{\pi} \frac{dy_c}{dx} d\theta \\ A_n &= \frac{2}{\pi} \int_0^{\pi} \frac{dy_c}{dx} \cos n\theta d\theta \end{aligned} \right\} \quad (9)$$

The lift force may be found from

$$\begin{aligned} {}_0L &= \int_0^c \rho V_0 \frac{d{}_0\Gamma}{dx} dx \\ &= c\rho V_0^2 \int_0^{\pi} \left[ A_0' (1 + \cos \theta) + A_0'' (1 - \cos \theta) \right. \\ &\quad \left. + \sum_1^{\infty} A_n \sin n\theta \sin \theta \right] d\theta \\ &= \pi c\rho V_0^2 \left( A_0' + A_0'' + \frac{1}{2} A_1 \right) \end{aligned}$$

so that the lift coefficient is

$$c c_l = 2\pi \left( A_0' + A_0'' + \frac{1}{2} A_1 \right) \quad (10)$$

According to theoretical hydrodynamics, in an inviscid fluid a strut section with a rounded trailing edge should experience no net lift at any angle of attack so that in this case

$$A_0'' = -\frac{1}{2} A_1 - A_0' \quad (11)$$

whence the relations (9) become

$$\left. \begin{aligned} A_0' &= \frac{1}{2} \left[ \alpha - \frac{1}{\pi} \int_0^{\pi} \frac{dy_c}{dx} (1 + \cos \theta) d\theta \right] \\ A_0'' &= -\frac{1}{2} \left[ \alpha - \frac{1}{\pi} \int_0^{\pi} \frac{dy_c}{dx} (1 - \cos \theta) d\theta \right] \\ A_n &= \frac{2}{\pi} \int_0^{\pi} \frac{dy_c}{dx} \cos n\theta d\theta \end{aligned} \right\} \quad (12)$$

In the case of an airfoil wherein the trailing edge is sharp, the "Kutta condition" must be satisfied (i. e., the flow must leave the trailing edge smoothly). To attain this the vorticity at the trailing edge must be zero, which requires that  $A_0'' = 0$ . So the coefficients become

$$\left. \begin{aligned} A_0' &= \alpha - \frac{1}{\pi} \int_0^{\pi} \frac{dy_c}{dx} d\theta \\ A_0'' &= 0 \\ A_n &= \frac{2}{\pi} \int_0^{\pi} \frac{dy_c}{dx} \cos n\theta d\theta \end{aligned} \right\} \quad (13)$$

It will be noted that for airfoils only  $A_0'$  and for struts only  $A_0'$  and  $A_0''$  vary with the angle of attack. The

coefficients  $A_n$  are independent of the angle of attack and are functions of the mean camber-line shape only.

Denote by  ${}_0P$  the difference at  $x$  between the upper and lower surface pressure coefficients,  $P_i - P_u$ . (The pressure coefficient is the pressure in terms of  $q$ , the stream dynamic pressure.) Then, from the Kutta-Joukowski theorem of lift,

$${}_0P = \frac{\rho V_0 \frac{d_0 \Gamma}{dx}}{q} = \frac{2}{V_0} \frac{d_0 \Gamma}{dx} \quad (14)$$

so that, from equation (4),

$${}_0P = 4 \left( A_0' \cot \frac{1}{2} \theta + A_0'' \tan \frac{1}{2} \theta + \sum_1^{\infty} A_n \sin n\theta \right) \quad (15)$$

It has been found convenient in the past to denote that part of the chordwise lift distribution which is in magnitude independent of the angle of attack and in form dependent solely upon the camberline shape, as the basic lift distribution; and that which is in magnitude variable with the angle of attack and in form independent of the mean camber-line shape, as the additional lift distribution. (These concepts first appeared in reference 6 and were later used in the development of the methods of references 7 and 8.) Hence, for the infinitesimally thin airfoil or strut the additional lift distribution is given by

$${}_0P_a = 4 \left( A_0' \cot \frac{1}{2} \theta + A_0'' \tan \frac{1}{2} \theta \right) \quad (16)$$

and the basic, by

$${}_0P_b = 4 \sum_1^{\infty} A_n \sin n\theta \quad (17)$$

It is convenient to consider the basic lift distribution only as characteristic of a given camber-line shape since the additional distribution may be modified at will by a change in the angle of attack and so, at some angle, must be zero. The angle of attack at which the magnitude of the additional distribution is zero for an airfoil is called the ideal angle  $\alpha_i$ , (references 6 and 9), and is given by

$$\alpha_i = \frac{1}{\pi} \int_0^{\pi} \frac{dy_c}{dx} d\theta \quad (18)$$

The ordinates of the mean camber line corresponding to the case when the additional distribution is zero, denoted by  $y_{c_0}$ , are related to the ordinates  $y_c$  by

$$\frac{y_{c_0}}{c} = \frac{y_c}{c} - \frac{x}{c} \alpha_i \quad (19)$$

and so

$$\frac{dy_{c_0}}{dx} = \frac{dy_c}{dx} - \alpha_i \quad (20)$$

From equations (8) and (17), then

$$\frac{dy_{c_0}}{dx} = \sum_1^{\infty} A_n \cos n\theta$$

and 
$$\frac{{}_0P_b}{4} = \sum_1^{\infty} A_n \sin n\theta \quad (21)$$

and the coefficients are given by

$$A_n = \frac{2}{\pi} \int_0^{\pi} \frac{dy_{c_0}}{dx} \cos n\theta d\theta = \frac{2}{\pi} \int_0^{\pi} \frac{{}_0P_b}{4} \sin n\theta d\theta \quad (22)$$

Using equations (21) and (22), the chordwise lift distribution corresponding to a given mean camber line or the mean camber line corresponding to a given chordwise lift distribution can be found. The calculations will in the general case be very lengthy so that it is desirable to replace the Fourier expansions by integral expressions, as was done in the development of the method of reference 1. To this end, the expression for the Fourier coefficients given by equation (22) can be substituted in equations (21). At  $\theta_0$  then

$$\left. \begin{aligned} \frac{{}_0P_{b_0}}{4} &= \frac{2}{\pi} \int_0^{\pi} \frac{dy_{c_0}}{dx} \sum_1^{\infty} \sin n\theta_0 \cos n\theta d\theta \\ \frac{dy_{c_0}}{dx} &= \frac{2}{\pi} \int_0^{\pi} \frac{{}_0P_b}{4} \sum_1^{\infty} \sin n\theta \cos n\theta_0 d\theta \end{aligned} \right\} \quad (23)$$

Now,

$$\sin n\theta_0 \cos n\theta = \frac{1}{2} [\sin n(\theta + \theta_0) - \sin n(\theta - \theta_0)]$$

$$\sin n\theta \cos n\theta_0 = \frac{1}{2} [\sin n(\theta + \theta_0) + \sin n(\theta - \theta_0)]$$

and further

$$\sum_1^{\infty} \sin n(\theta \pm \theta_0) = \frac{1}{2} \cot \left( \frac{\theta \pm \theta_0}{2} \right) - \frac{\cos (2n+1) \left( \frac{\theta \pm \theta_0}{2} \right)}{2 \sin \left( \frac{\theta \pm \theta_0}{2} \right)}$$

so that substitution gives

$$\begin{aligned} \frac{{}_0P_{b_0}}{4} &= \lim_{n \rightarrow \infty} \left\{ \frac{1}{2\pi} \int_0^{\pi} \frac{dy_{c_0}}{dx} \left[ \cot \left( \frac{\theta + \theta_0}{2} \right) - \cot \left( \frac{\theta - \theta_0}{2} \right) \right] d\theta - \right. \\ &\left. \frac{1}{2\pi} \int_0^{\pi} \frac{dy_{c_0}}{dx} \left[ \frac{\cos (2n+1) \left( \frac{\theta + \theta_0}{2} \right)}{\sin \left( \frac{\theta + \theta_0}{2} \right)} - \frac{\cos (2n+1) \left( \frac{\theta - \theta_0}{2} \right)}{\sin \left( \frac{\theta - \theta_0}{2} \right)} \right] d\theta \right\} \end{aligned}$$

and

$$\begin{aligned} \frac{dy_{c_0}}{dx} &= \lim_{n \rightarrow \infty} \left\{ \frac{1}{2\pi} \int_0^{\pi} \frac{{}_0P_b}{4} \left[ \cot \left( \frac{\theta + \theta_0}{2} \right) + \cot \left( \frac{\theta - \theta_0}{2} \right) \right] d\theta - \right. \\ &\left. \frac{1}{2\pi} \int_0^{\pi} \frac{{}_0P_b}{4} \left[ \frac{\cos (2n+1) \left( \frac{\theta + \theta_0}{2} \right)}{\sin \left( \frac{\theta + \theta_0}{2} \right)} + \frac{\cos (2n+1) \left( \frac{\theta - \theta_0}{2} \right)}{\sin \left( \frac{\theta - \theta_0}{2} \right)} \right] d\theta \right\} \end{aligned}$$

In the limit, the second integrals in the above relations become zero so that the equations may be written as

$$\left. \begin{aligned} \frac{{}_0P_{b_0}}{4} &= \frac{1}{2\pi} \int_0^{\pi} \frac{dy_{c_0}}{dx} \left[ \cot \left( \frac{\theta + \theta_0}{2} \right) - \cot \left( \frac{\theta - \theta_0}{2} \right) \right] d\theta \\ \frac{dy_{c_0}}{dx} &= \frac{1}{2\pi} \int_0^{\pi} \frac{{}_0P_b}{4} \left[ \cot \left( \frac{\theta + \theta_0}{2} \right) + \cot \left( \frac{\theta - \theta_0}{2} \right) \right] d\theta \end{aligned} \right\} \quad (24)$$

When either function is known in simple algebraic form, it is sometimes convenient to express these integrals as

follows: From known trigonometric relations, equations (24) may be written

$$\left. \begin{aligned} \frac{{}_0P_{b_0}}{4} &= \frac{1}{\pi} \int_0^\pi \frac{dy_{c_b}}{dx} \frac{\sin \theta d\theta}{\cos \theta - \cos \theta_0} \\ \frac{dy_{c_{b_0}}}{dx} &= -\frac{1}{\pi} \int_0^\pi \frac{{}_0P_b}{4} \frac{\sin \theta d\theta}{\cos \theta - \cos \theta_0} \end{aligned} \right\} \quad (25)$$

which may be useful if the functions under the integrals are expressed as simple functions of  $\theta$ .

When the functions are expressed in terms of  $x$ , the following forms, obtained by substituting the relations of  $x$  with  $\theta$  given by equation (3), are sometimes useful:

$$\left. \begin{aligned} \frac{{}_0P_{b_0}}{4} &= -\frac{1}{\pi} \int_0^c \frac{dy_{c_b}}{dx} \frac{\sqrt{x_0(c-x)}}{(x-x_0)\sqrt{x(c-x)}} dx \\ \frac{dy_{c_{b_0}}}{dx} &= \frac{1}{\pi} \int_0^c \frac{{}_0P_b dx}{4(x-x_0)} \end{aligned} \right\} \quad (26)$$

The second equation has been used to determine the shape of a variety of camber lines, notably the type "a" mean camber lines (reference 9) used with the more common low-drag and high-critical-compressibility-speed airfoils.

Unless the algebraic expressions for  ${}_0P_b$  or  $dy_c/dx$  are very simple, the direct integrations using equations (25) and (26) are not convenient so that, in general, it is desirable to perform the integrations numerically using equations (24).

The computation may be shortened considerably by use of the following mathematical device:

$$\int_0^\pi f(\theta) \cot\left(\frac{\theta+\theta_0}{2}\right) d\theta = -\int_\pi^{2\pi} f(2\pi-\theta) \cot\left(\frac{\theta-\theta_0}{2}\right) d\theta$$

Hence, equations (24) may be written

$$\left. \begin{aligned} \frac{{}_0P_{b_0}}{4} &= -\frac{1}{2\pi} \int_0^{2\pi} \frac{dy_{c_b}}{dx} \cot\left(\frac{\theta-\theta_0}{2}\right) d\theta, \\ \text{defining } \left(\frac{dy_{c_b}}{dx}\right)_{\pi+\theta} &= \left(\frac{dy_{c_b}}{dx}\right)_{\pi-\theta} \\ \frac{dy_{c_{b_0}}}{dx} &= \frac{1}{2\pi} \int_0^{2\pi} \frac{{}_0P_b}{4} \cot\left(\frac{\theta-\theta_0}{2}\right) d\theta, \\ \text{defining } \left(\frac{{}_0P_b}{4}\right)_{\pi+\theta} &= -\left(\frac{{}_0P_b}{4}\right)_{\pi-\theta} \end{aligned} \right\} \quad (27)$$

These integrals may be evaluated numerically by the method of reference 1 which is given in Appendix A of this report.

In the preceding theory it was assumed that the airfoil was of infinitesimal thickness, hence the velocity at each elemental vortex along the camber line was taken to be the free-stream velocity  $V_0$ . For airfoils of finite thickness, the velocity differs somewhat from  $V_0$ . A better approximation is to assume that the velocity at each vortex is the velocity on the surface of the base profile at the same station. Hence,

the effect of airfoil thickness will be to change the local lift at  $x$  to approximately

$$P = {}_0P \left( \frac{V_f}{V_0} \right) \quad (28)$$

where  $V_f$  is the local velocity on the base profile at  $x$ . The calculation of  $V_f$  is considered later in this report.

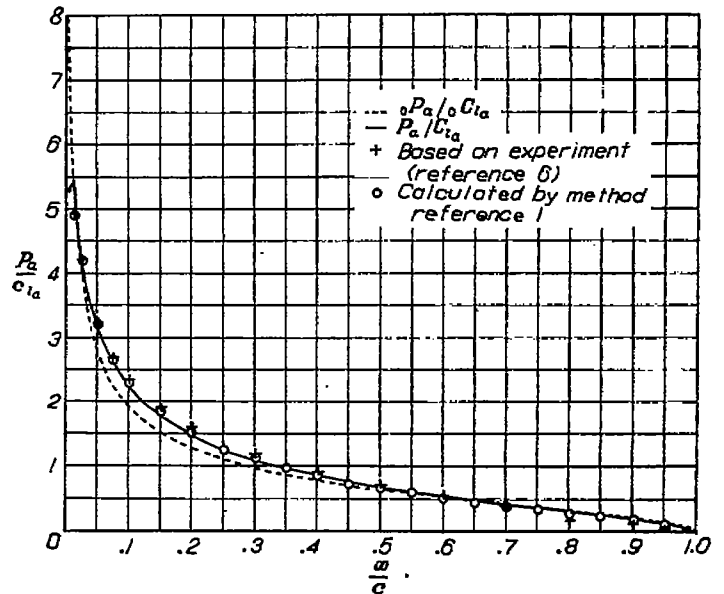


FIGURE 2.—Additional lift distribution for NACA 0012 airfoil.

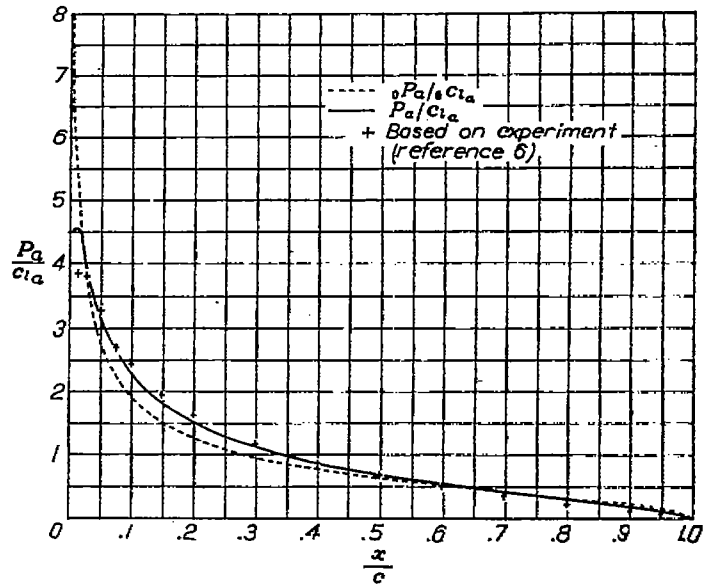


FIGURE 3.—Additional lift distribution for NACA 0018 airfoil.

Values of  $P_a/c_{l\alpha}$  calculated by equation (28) for the NACA 0012 and 0018 airfoils are shown in figures 2 and 3, respectively, along with the values given by the method of reference 7 which were obtained by interpolation of experimental pressure distributions. Shown dotted are the theoretical values  ${}_0P_a/c_{l\alpha}$  for the infinitesimally thin airfoil obtained from equation (16) and given in table I. In figure 4 the calculated and experimental basic lift distributions for the

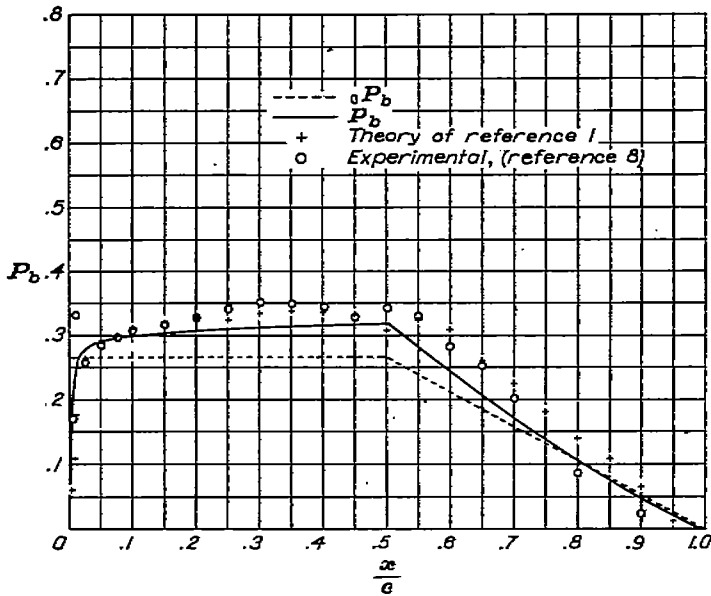


FIGURE 4.—Basic lift distribution for NACA 35-215 low-drag airfoil.

$\alpha=0.5$  mean camber line of the NACA 35-215 airfoil are shown. It is evident from these figures that equation (28) gives a close second approximation to the value of  $P$ .

The basic lift coefficient becomes

$$c_{l_0} = \int_0^1 P_b \left( \frac{V_f}{V_0} \right) d \left( \frac{x}{c} \right) \quad (29)$$

and the quarter-chord moment coefficient is

$$c_{m_{0.25}} = \int_0^1 P_b \left( \frac{V_f}{V_0} \right) \left( \frac{1}{4} - \frac{x}{c} \right) d \left( \frac{x}{c} \right) \quad (30)$$

It is obviously inconsistent to make the approximate velocity correction to the lift distribution (equation (28)) and not to the velocity ratio  $v/V_0$  in equation (2). However, the correction to the lift distribution accounts for nearly all the discrepancies between the calculated and experimental results so that the additional computational dif-

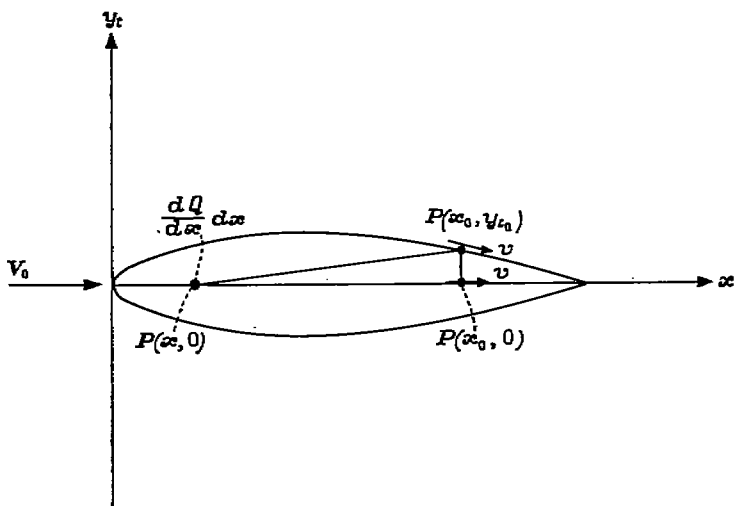


FIGURE 5.—Diagram of base profile.

ficulties associated with a further improvement of the theory are not considered to be justified.

BASE-PROFILE THEORY

The problem of determining the velocity distribution over a given base profile or the base profile which will promote a given velocity distribution over its surface may be treated in a manner analogous to that of the mean-camber-line theory.

Consider the base profile shown in figure 5. If the thickness is small, the velocity induced at a point  $P(x_0, y_{t0})$  on the surface of the profile by a fluid source or sink at the point  $P(x, 0)$  is approximately that which would be induced at the point  $P(x_0, 0)$  by this source or sink. If the source strength at a point  $x$  is  $(dQ/dx)dx$ , then, the velocity induced by all sources or sinks distributed along the  $x$ -axis will be

$$v(x_0) = \frac{1}{2\pi} \int_0^c \frac{dQ}{dx} \frac{dx}{x_0 - x} \quad (31)$$

The source strength can be related to the shape in the following approximate manner: If the profile is thin, the velocity at the surface does not differ materially from the free-stream velocity  $V_0$ , and hence the flow velocity within the profile due to the sources and sinks is as a first approximation  $V_0$ . Within the profile the difference between the quantity of fluid flowing at  $x+dx$  and  $x$  is the amount supplied by the source contained within this interval, hence

$$\frac{dQ}{dx} dx \approx 2V_0 \left( y_t + \frac{dy_t}{dx} dx \right) - 2V_0 y_t$$

so

$$\frac{dQ}{dx} = 2V_0 \frac{dy_t}{dx} \quad (32)$$

and so equation (31) become approximately

$$\frac{v}{V_0} = \frac{1}{\pi} \int_0^c \frac{dy_t}{dx} \frac{dx}{x_0 - x} \quad (33)$$

Replacing  $x$  by the  $\theta$  coordinate defined by equation (3) and assuming that the slope of the profile is given by

$$\frac{dy_t}{dx} = B_0' \cot \frac{1}{2}\theta + B_0'' \tan \frac{1}{2}\theta + \sum_1^{\infty} B_n \sin n\theta \quad (34)$$

then by analogy with the similar development in the mean camber-line theory

$$\frac{v}{V_0} = B_0' - B_0'' - \sum_1^{\infty} B_n \cos n\theta \quad (35)$$

and

$$\left. \begin{aligned} B_0' - B_0'' &= \frac{1}{\pi} \int_0^{\pi} \frac{v}{V_0} d\theta \\ B_n &= -\frac{2}{\pi} \int_0^{\pi} \frac{v}{V_0} \cos n\theta d\theta \end{aligned} \right\} \quad (36)$$

The condition that the trailing edge shall close is given by

$$\int_0^{\pi} dy_t = \int_0^{\pi} \frac{dy_t}{dx} dx = 0$$

Substituting the slope as given by equation (34) and integrating, it is found that

$$B_0' + B_0'' + \frac{1}{2} B_1 = 0 \tag{37}$$

It is of interest to note that setting all coefficients except  $B_0'$  and  $B_0''$  equal to zero then requires

$$B_0'' = -B_0'$$

Hence

$$\frac{dy_t}{dx} = B_0' \left( \cot \frac{1}{2} \theta - \tan \frac{1}{2} \theta \right)$$

which becomes after integration,

$$y = cB_0' \sin \theta$$

or

$$y = 2cB_0' \sqrt{\frac{x}{c} \left( 1 - \frac{x}{c} \right)}$$

This is the equation of an ellipse of thickness

$$t = 2cB_0'$$

The induced velocity from equation (35) is

$$\frac{v}{V_0} = 2B_0' = \frac{t}{c}$$

so that adding this induced velocity to the stream velocity  $V_0$ , the ratio of the local velocity at any station  $x$  to the stream velocity is found to be

$$\frac{V_f}{V_0} = 1 + \frac{t}{c} \tag{38}$$

Again, if all coefficients except  $B_0'$  and  $B_1$  are set equal to zero, then from equation (37)

$$B_1 = -2B_0'$$

Hence

$$\frac{dy_t}{dx} = B_0' \left( \cot \frac{1}{2} \theta - 2 \sin \theta \right)$$

which becomes, after integration,

$$y = \frac{cB_0'}{2} \sin \theta (1 + \cos \theta)$$

or

$$y = 2cB_0' \left( 1 - \frac{x}{c} \right)^{\frac{1}{2}} \sqrt{\frac{x}{c}}$$

This is the approximate equation for a thin Joukowski base profile of thickness

$$t = \frac{3\sqrt{3} B_0' c}{4}$$

The induced velocity from equation (35) is then

$$\frac{v}{V_0} = B_0' (1 + 2 \cos \theta) = \frac{4}{3\sqrt{3}} \left( \frac{t}{c} \right) \left[ 3 - 4 \left( \frac{x}{c} \right) \right]$$

Hence, the ratio of the local to stream velocity is

$$\frac{V_f}{V_0} = 1 + \frac{4}{3\sqrt{3}} \left( \frac{t}{c} \right) \left[ 3 - 4 \left( \frac{x}{c} \right) \right] \tag{39}$$

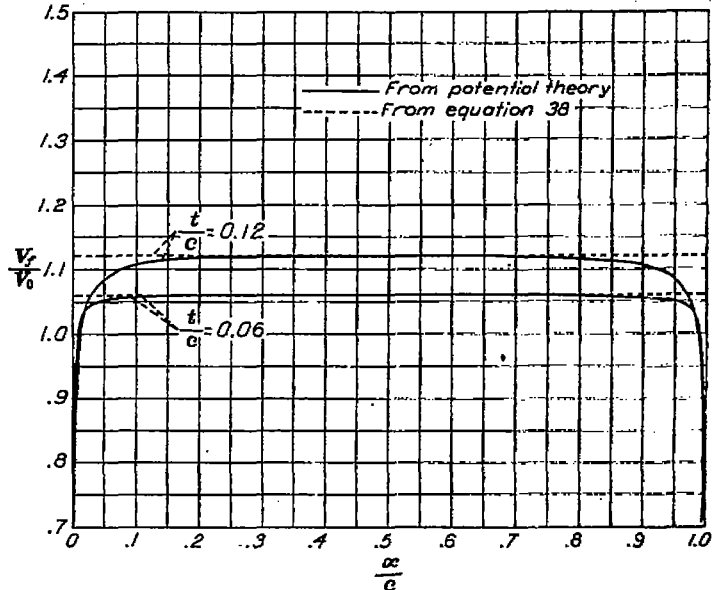


FIGURE 6.—Theoretical velocity distribution over elliptic base profiles.

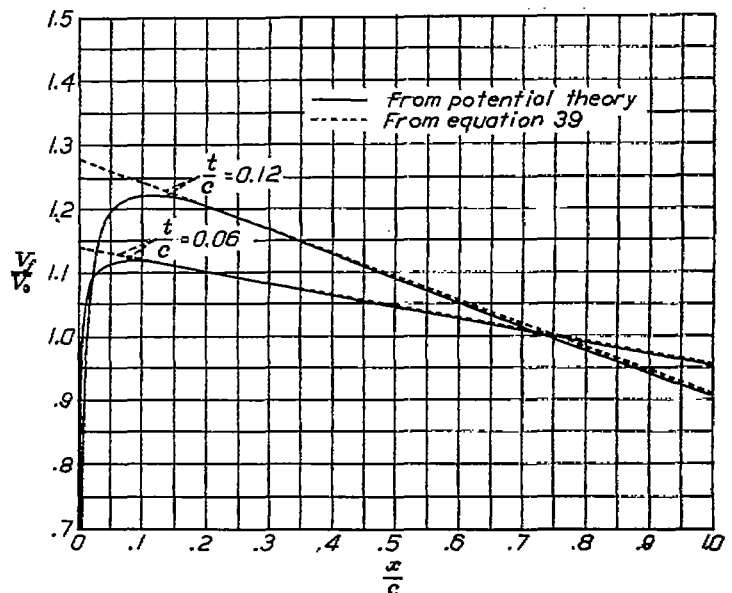


FIGURE 7.—Theoretical velocity distribution over Joukowski base profiles.

The velocity distribution for the elliptic base profile as calculated by equation (38), and for the Joukowski base profile as calculated by equation (39) is shown in figures 6 and 7, respectively, along with theoretically correct velocity distributions as calculated from potential theory. It is seen that the approximate velocity distributions are satisfactory except in the region where the slope  $dy_t/dx$  becomes infinite. This was to be expected since the assumptions made in the

development of the theory in effect require that  $dy_i/dx$  be small. Inaccuracies due to such infinite slopes may be avoided by the following device: It is evident from equations (34) and (35) that superposition is permissible in regard to both base-profile shapes and the corresponding induced velocities. Hence the method may be used to find the change in shape corresponding to a specified change in velocity distribution or, inversely, the change in velocity distribution corresponding to a specified change in shape from some "reference base profile." If this reference base profile is one properly chosen so as to have the same slope characteristics at the leading and trailing edges as has the profile under consideration, then the  $B_0'$  and  $B_0''$  coefficients in the series to represent such changes can be made zero since now slope differences need never become infinite. For example, for an airfoil with rounded leading edge and pointed trailing edge, the Joukowski base profile having the same leading-edge radius may be used as the reference base profile; for a strut with rounded leading and trailing edges, the elliptic base profile having the same leading- and trailing-edge radii may be used as the reference base profile. Letting  $\Delta y_i$  and  $\Delta v$  represent the change in shape and velocity, respectively, then equations (34) and (35) become

$$\left. \begin{aligned} \frac{d(\Delta y_i)}{dx} &= \sum_1^{\infty} B_n \sin n\theta \\ \frac{\Delta v}{V_0} &= -\sum_1^{\infty} B_n \cos n\theta \end{aligned} \right\} \quad (40)$$

and the coefficients are

$$\left. \begin{aligned} B_n &= \frac{2}{\pi} \int_0^{\pi} \frac{d(\Delta y_i)}{dx} \sin n\theta \, d\theta \\ \text{or} \\ B_n &= -\frac{2}{\pi} \int_0^{\pi} \frac{\Delta v}{V_0} \cos n\theta \, d\theta \end{aligned} \right\} \quad (41)$$

Since  $B_0'$  and  $B_0''$  have been set equal to zero, then from equation (37) the coefficient  $B_1$  must also be zero.

When it is desired to find the change in the velocity distribution corresponding to some given change in shape, the given change in shape—if so chosen that  $d(\Delta y_i)/dx$  is not infinite at the leading and trailing edges—automatically satisfies the condition that the coefficients  $B_0'$ ,  $B_0''$ , and  $B_1$  are zero. However, when it is desired to find the change in base-profile shape corresponding to a given change in the velocity distribution, the change in velocity distribution must be so chosen that

$$\text{and} \quad \left. \begin{aligned} \int_0^{\pi} \frac{\Delta v}{V_0} \, d\theta &= 0 \\ \int_0^{\pi} \frac{\Delta v}{V_0} \cos \theta \, d\theta &= 0 \end{aligned} \right\} \quad (42)$$

if the velocity distribution chosen is to correspond to a real base profile.

As shown in the preceding theory of the mean camber line, the sine and cosine series can be replaced by the integral relations which are generally superior for purposes of computa-

tion. Where the change in shape or velocity distribution is known as a relatively simple trigonometric function in  $\theta$ , it is sometimes convenient to use the equations

$$\text{and} \quad \left. \begin{aligned} \frac{d(\Delta y_i)}{dx} &= -\frac{1}{\pi} \int_0^{\pi} \frac{\Delta v}{V_0} \frac{\sin \theta \, d\theta}{\cos \theta - \cos \theta_0} \\ \frac{\Delta v_0}{V_0} &= \frac{1}{\pi} \int_0^{\pi} \frac{d(\Delta y_i)}{dx} \frac{\sin \theta \, d\theta}{\cos \theta - \cos \theta_0} \end{aligned} \right\} \quad (43)$$

When the change in shape or velocity distribution is known as a relatively simple function of  $x$ , then it is sometimes convenient to use the equations

$$\left. \begin{aligned} \frac{d(\Delta y_i)}{dx} &= \frac{1}{\pi} \int_0^c \frac{\Delta v}{V_0} \frac{\sqrt{x_0(c-x_0)}}{\sqrt{x(c-x)}} \, dx \\ \frac{\Delta v_0}{V_0} &= -\frac{1}{\pi} \int_0^c \frac{d(\Delta y_i)}{dx} \frac{dx}{x-x_0} \end{aligned} \right\} \quad (44)$$

In the general case when the equations for  $\Delta v/V_0$  and  $d(\Delta y_i)/dx$  are complex or unknown, the most useful forms of the equations are

$$\left. \begin{aligned} \frac{d(\Delta y_i)}{dx} &= \frac{1}{2\pi} \int_0^{2\pi} \frac{\Delta v}{V_0} \cot \left( \frac{\theta - \theta_0}{2} \right) \, d\theta, \\ \text{defining} \left( \frac{\Delta v}{V_0} \right)_{r+\theta} &= \left( \frac{\Delta v}{V_0} \right)_{r-\theta} \\ \frac{\Delta v_0}{V_0} &= \frac{1}{2\pi} \int_0^{2\pi} \frac{d(\Delta y_i)}{dx} \cot \left( \frac{\theta - \theta_0}{2} \right) \, d\theta, \\ \text{defining} \left[ \frac{d(\Delta y_i)}{dx} \right]_{r+\theta} &= - \left[ \frac{d(\Delta y_i)}{dx} \right]_{r-\theta} \end{aligned} \right\} \quad (45)$$

These integrals can be evaluated numerically by the method given in Appendix A.

### APPLICATIONS OF THE METHOD

#### THE CALCULATION OF THE VELOCITY DISTRIBUTION OVER A GIVEN AIRFOIL SECTION

In this section the procedure to be followed to calculate the velocity distribution over a given airfoil section is presented, and the calculation of the velocity distribution over the NACA 4412 airfoil section is used as an example.

The procedure may be summarized as follows: The ordinates of the base profile are obtained from the airfoil ordinates by removing the camber. The velocity distribution over the base profile is found by adding to the known velocity distribution over some reference base profile having the same leading-edge radius, the change in the velocity distribution due to a change in shape from the reference to the given base profile. Next, the ordinates of the camber line are obtained from the airfoil ordinates by removing the thickness. The chordwise lift distribution over this infinitesimally thin camber line is calculated and corrected for the effect of thickness. Finally, the effect of camber is combined with the velocity distribution over the base profile to give the velocity distribution over the given airfoil section.

From the known airfoil section, the ordinates  $y_x$ , the nose radius of the base profile  $r_{L.E.}/c$ , and the ordinates of the mean camber line  $y_c/c$  are determined for some or all of the standard stations  $x/c$  listed in table V. In the general case this may be done graphically from a large plot of the airfoil, taking care to measure the base-profile ordinates perpendicular to the mean camber line at each station. All modern NACA conventional and low-drag airfoils are formed from specified base profiles and mean camber lines, and the ordinates or equations for the ordinates can be found in NACA reports. For the NACA 4412 airfoil, the ordinate of the base profile (i. e., the NACA 0012) and the equation for the ordinates of the camber line are given in reference 10.

The base-profile velocity distribution is calculated as follows: A reference base profile having approximately the same nose radius is chosen from the Joukowski profiles listed in table II. The thickness ratio of a Joukowski profile having the leading-edge radius  $r_{L.E.}$  is

$$\frac{t}{c} = 0.918 \sqrt{\frac{r_{L.E.}}{c}} \quad (51)$$

For the NACA 4412, the leading-edge radius is  $0.0158c$ , the proper thickness ratio for the Joukowski base profile is then  $0.1155$ . It is sufficiently exact and more convenient to use the Joukowski section with  $t/c = 0.12$ . The difference between the ordinates of the given and reference profile is found from

$$\frac{\Delta y_t}{c} = \frac{y_t}{c} - \frac{y_{t_r}}{c} \quad (52)$$

and listed as in table III. These difference ordinates are plotted as a function of  $x/c$ , as in figure 8, and the slopes graphically determine. These slopes are plotted as functions of  $\theta$  in radians (fig. 9) with the slopes at  $\theta = 0$  and  $\theta = \pi$  arbitrarily set equal to zero. Then the ordinates and slopes at the proper  $\theta$  stations given in the Appendix A for the numerical integration of equation (45) are found and listed

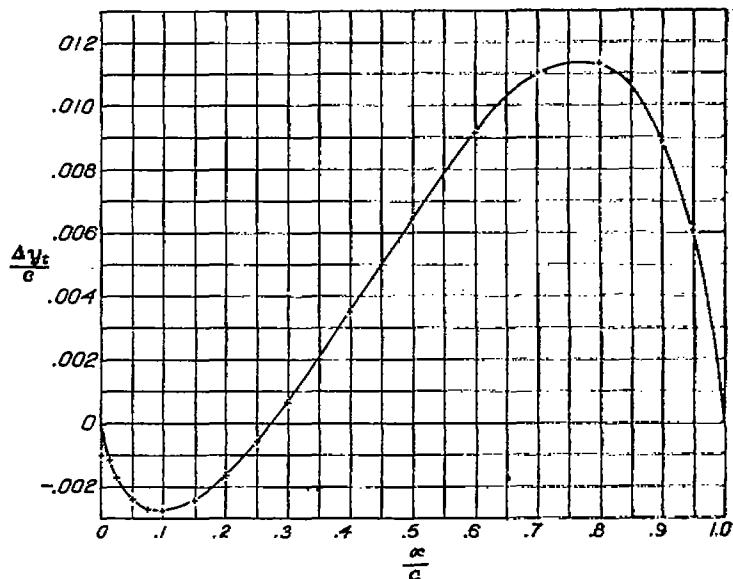


FIGURE 8.—Difference ordinates for base profile of NACA 4412 airfoil section as a function of  $x/c$ .

in table IV. (Note that the value of the ordinate at station  $\pi + \theta$  must be taken as the value at  $\pi - \theta$  but with opposite sign.) If the curve of figure 9 is fair, the "20-point" method of integration, used in the example, is sufficiently exact. The integration is performed as illustrated in Appendix A. The resulting values of  $\Delta v/V_0$  are plotted as a function of  $x/c$  using the conversion table V, and the values at the standard stations, taken from this curve, are listed as in table III. The velocity distribution over the base profile is found from

$$\frac{V_f}{V_0} = \frac{V_r}{V_0} + \frac{\Delta v}{V_0} \quad (53)$$

where the values of  $V_r/V_0$  are those for the reference profile given in table II. For comparison, these calculated values have been plotted in figure 10 to an expanded scale of  $V_f/V_0$  along with those determined by the [method] of reference 1.

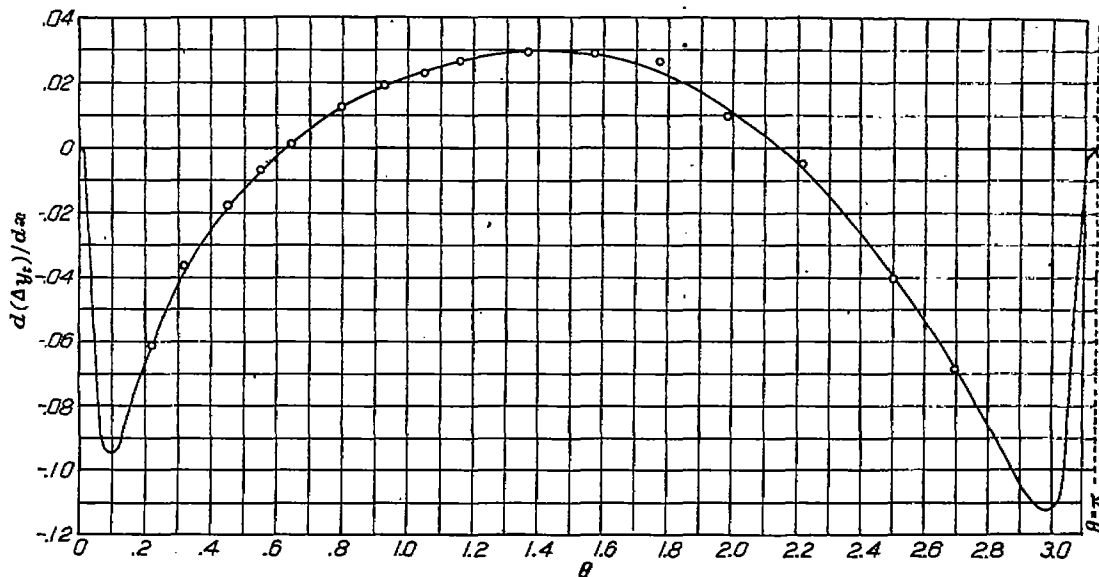


FIGURE 9.—Slope of the difference ordinates for base profile of NACA 4412 airfoil section as a function of  $\theta$ .

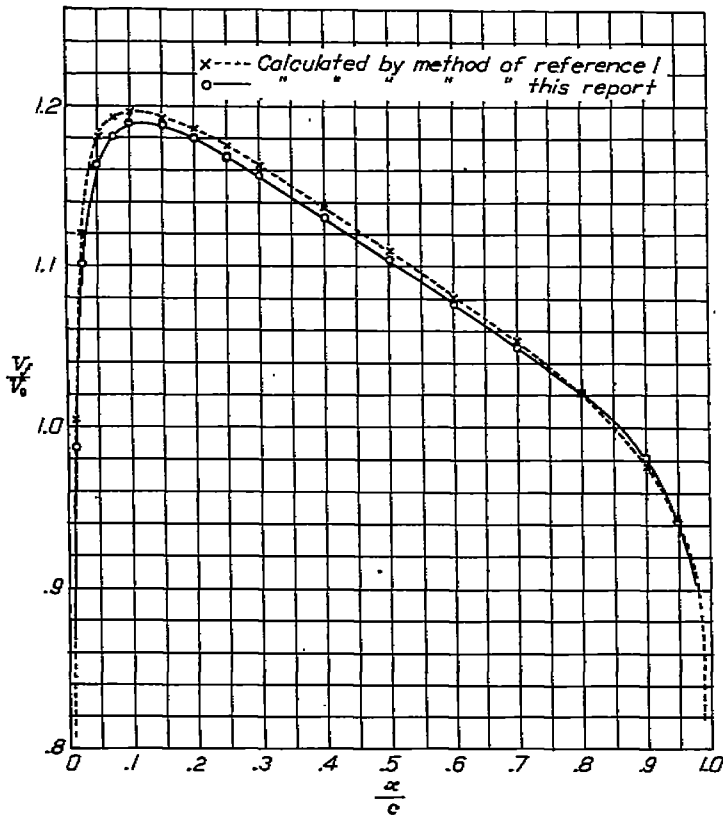


FIGURE 10.—Velocity distribution over NACA 4412 base profile.

The chordwise lift distribution is calculated, in general, as follows: From a curve of the mean-camber-line ordinates as a function of  $x/c$ , the slopes are determined and plotted as a function of  $\theta$ . From this graph, the ordinates and slopes are determined at the proper  $\theta$  stations given in Appendix A for the numerical integration of equation (27). (The values of ordinates at station  $\pi + \theta$  must be taken as the same in sign and magnitude as the values at station  $\pi - \theta$ .) The integration is performed to obtain the value of  ${}_0P_b$ .

For the mean camber line of the NACA 4412 airfoil, because the equation of the shape is given in elementary functions of  $x/c$ , the procedure may be simplified. From the leading edge to  $x/c=0.4$

$$\frac{y_c}{c} = \frac{1}{4} \left[ 0.8 \frac{x}{c} - \left( \frac{x}{c} \right)^2 \right]$$

and from  $x/c=0.4$  to  $x/c=1.0$

$$\frac{y_c}{c} = \frac{1}{9} \left[ 0.2 + 0.8 \frac{x}{c} - \left( \frac{x}{c} \right)^2 \right]$$

(It is to be noted that if  ${}_0P_b$  is found from the integral equations (25), (26), or (27), regardless of whether  $y_{c0}$  or  $y_c$  is used in the calculation, the additional distribution will not appear in the final answer.) Differentiation gives

$$\frac{dy_c}{dx} = \frac{1}{4} \left[ 0.8 - 2 \left( \frac{x}{c} \right) \right]; \quad 0 < \frac{x}{c} < 0.4$$

$$\frac{dy_c}{dx} = \frac{1}{9} \left[ 0.8 - 2 \left( \frac{x}{c} \right) \right]; \quad 0.4 < \frac{x}{c} < 1.0$$

Using equation (3), these may be written in terms of  $\theta$  as

$$\frac{dy_c}{dx} = \frac{1}{4} (\cos \theta - 0.2); \quad 0 < \theta < \cos^{-1}(0.2)$$

$$\frac{dy_c}{dx} = \frac{1}{9} (\cos \theta - 0.2); \quad \cos^{-1}(0.2) < \theta < \pi$$

These relations could be employed directly in equation (25) and the lift distribution obtained. The existence of the singular point, however, makes the algebra tedious.

To employ the numerical method of integration, the slopes  $d/d\theta$  ( $dy_c/dx$ ), may be obtained by differentiation of the above.

$$\frac{d}{d\theta} \left( \frac{dy_c}{dx} \right) = -\frac{1}{4} \sin \theta \quad 0 < \theta < \cos^{-1}(0.2)$$

$$\frac{d}{d\theta} \left( \frac{dy_c}{dx} \right) = -\frac{1}{9} \sin \theta \quad \cos^{-1}(0.2) < \theta < \pi$$

Using the above equations, the ordinates and slopes of the curve of  $dy_c/dx$  as a function of  $\theta$  can be calculated directly for the proper  $\theta$  stations used in the numerical integration (table VI) and the integration performed. The values of  ${}_0P_b$  are then plotted as functions of  $x/c$  (fig. 11) and the values obtained for the standard stations. These values apply to an airfoil of infinitesimal thickness, and the values must be corrected to correspond to the airfoil of finite thickness (loc. cit. equation (28)) by use of the equation (table VII)

$$P_b = \left( \frac{V_f}{V_0} \right) {}_0P_b \quad (54)$$

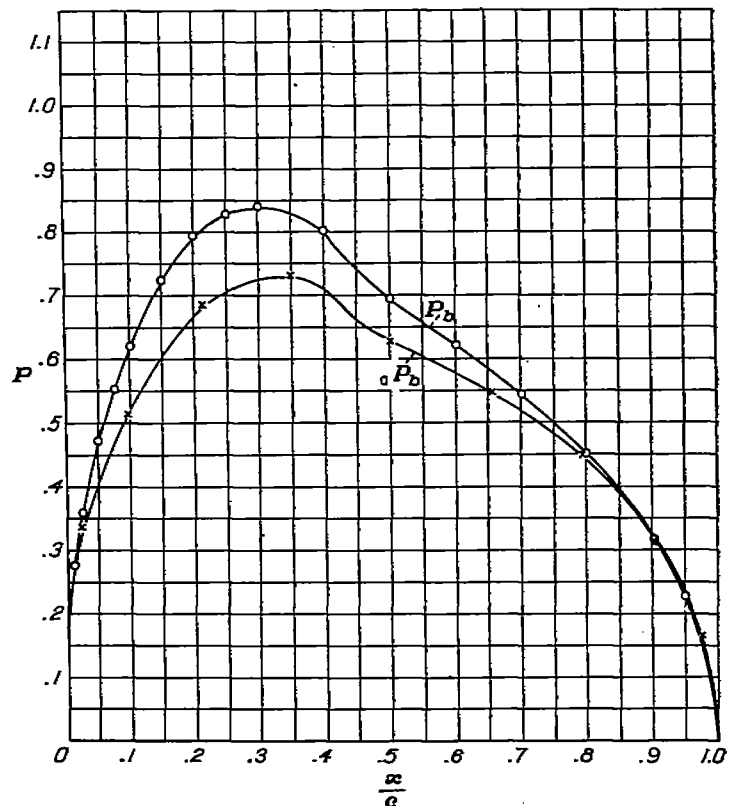


FIGURE 11.—Calculated basic lift distribution for NACA 4412 airfoil section.

These values are also plotted as in figure 11. The basic or ideal lift coefficient is then determined from an integration of the plot of  $P_b$  as a function of  $x/c$ .

The additional distribution can be calculated by finding first the values of  $P_a$  for  ${}_0c_{i_a}$  of unity from

$$P_a({}_0c_{i_a}=1) = \left(\frac{V_f}{V_0}\right) \left(\frac{{}_0P_a}{{}_0c_{i_a}}\right) \quad (55)$$

using the values of  $({}_0P_a/{}_0c_{i_a})$  from table I. This function is plotted and the integral  $c_{i_a}({}_0c_{i_a}=1)$  is determined. Then the additional distribution is found from

$$\left(\frac{P_a}{c_{i_a}}\right) = \frac{P_a({}_0c_{i_a}=1)}{c_{i_a}({}_0c_{i_a}=1)} \quad (56)$$

as in table VII.

The chordwise lift distribution corresponding to a lift coefficient  $c_l$  can be found from

$$P = P_b + (c_l - c_{i_b}) \left(\frac{P_a}{c_{i_a}}\right) \quad (57)$$

The velocity distribution over the airfoil may be found by superposition method of reference 4. The upper and lower surface velocity distributions, respectively, are

$$\left. \begin{aligned} \frac{V_u}{V_0} &= \frac{V_f}{V_0} + \frac{P/4}{V_f/V_0} \\ \frac{V_l}{V_0} &= \frac{V_f}{V_0} - \frac{P/4}{V_f/V_0} \end{aligned} \right\} \quad (58)$$

and

$$\left. \begin{aligned} \frac{V_u}{V_0} &= \frac{V_f}{V_0} + \frac{P/4}{V_f/V_0} \\ \frac{V_l}{V_0} &= \frac{V_f}{V_0} - \frac{P/4}{V_f/V_0} \end{aligned} \right\}$$

In table VIII, the velocity-distribution calculations for the NACA 4412 at  $c_l=0.72$  are given. The calculated values

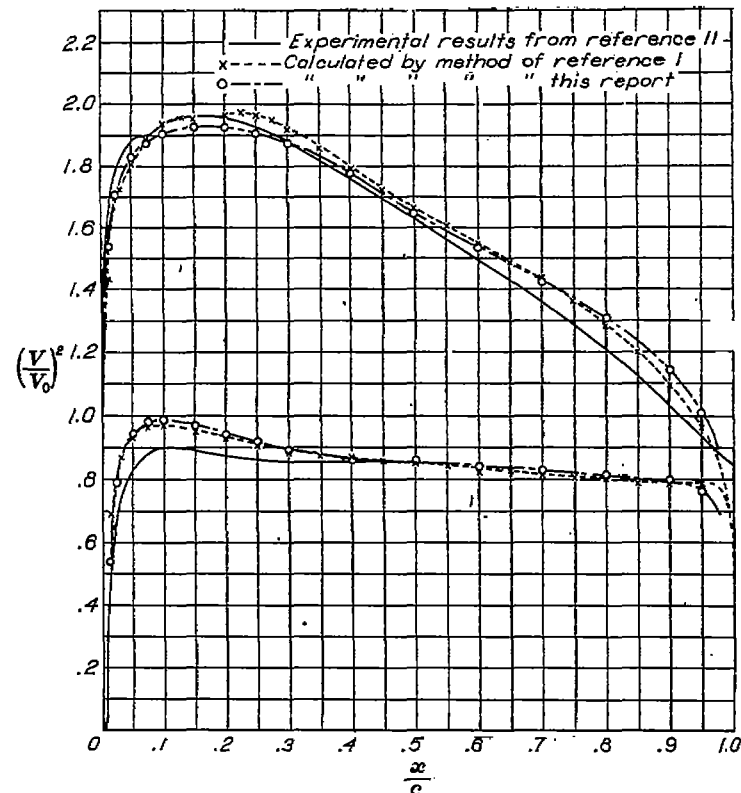


FIGURE 12.—Velocity distribution over NACA 4412 airfoil section at  $c_l=0.72$ .

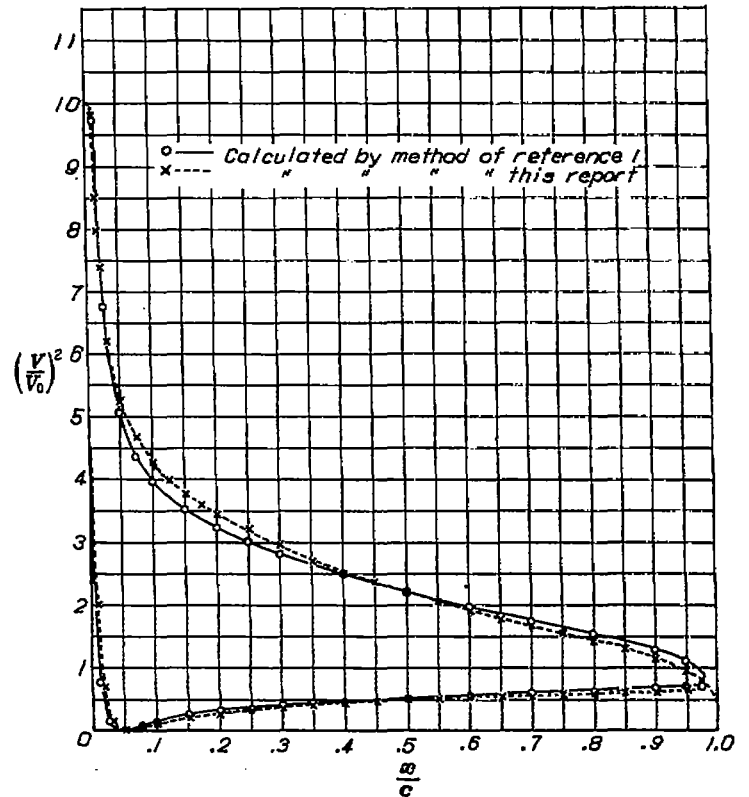


FIGURE 13.—Velocity distribution over NACA 4412 airfoil section at  $c_l=2.05$ .

of  $(V/V_0)^2$  are plotted in figure 12 along with the calculated values obtained by the method of reference 1. Also shown for comparison in the solid curve are experimental values obtained by interpolation of the experimental pressure distributions of reference 11.

In figure 13 are shown the calculated values of  $(V/V_0)^2$  for NACA 4412 at  $c_l=2.05$  as determined by the method of this report and of reference 1.

The procedure to be followed to calculate the velocity distribution over a strut section having a rounded trailing edge is the same as that for the airfoil, except that the reference profile must be one having both a rounded leading and trailing edge. The elliptic sections given in table IX are recommended for use as base profiles in these cases. Strut sections are usually not cambered, so that the procedure to be followed for cambered strut sections is only of academic interest and is accordingly not considered here. It may, however, be desirable to calculate the velocity distribution over a strut section at some angle of attack other than zero. In this case, the value of  ${}_0P_a$  is calculated from

$${}_0P_a = 2\alpha \left( \cot \frac{1}{2} \theta - \tan \frac{1}{2} \theta \right) \quad (59)$$

$$\text{or} \quad {}_0P_a = 2\alpha \left[ \frac{1 - 2\frac{x}{c}}{\sqrt{\frac{x}{c} \left(1 - \frac{x}{c}\right)}} \right]$$

and the lift distribution from

$$P_a = \left(\frac{V_f}{V_0}\right) {}_0P_a \quad (60)$$

With this lift distribution the integrated value of the lift coefficient may not be zero as required by the potential theory. A small shift of the distribution would allow this requirement to be met, but such a refinement is not justified in view of the fact that for real fluids, as a result of the fluid viscosity, this requirement is not actually fulfilled. Using the value of  $P_a$ , the velocity distribution over the strut is found from equations (58).

THE CALCULATION OF SHAPE OF AN AIRFOIL SECTION CORRESPONDING TO A GIVEN VELOCITY DISTRIBUTION

In this section the procedure to be followed to calculate the airfoil section shape corresponding to a desired velocity distribution is presented. To demonstrate the general procedure to be employed in the calculation of an airfoil shape corresponding to a desired velocity distribution, the shape of a "semi-low-drag" airfoil over which the maximum velocity occurs near the leading edge on the upper surface and at the midchord location on the lower surface is used as a first example. As a second example, the specific calculation of airfoil shapes having a "double-roof" type velocity distribution is considered.

It should be noted at the outset that the shape of a two-dimensional body corresponding to some desired velocity distribution may not represent a real airfoil section which is both "closed" and pointed at the trailing edge. As a consequence the desired velocity distribution can be considered only as a "first choice" and must be modified, if necessary, to satisfy these conditions. The procedure employed in adjusting the desired velocity distribution and calculating the shape of the corresponding airfoil is as follows: From the desired airfoil velocity distribution, the corresponding velocity distribution over the base profile is found by averaging the upper and lower surface velocities at each chordwise station. This distribution is examined to determine whether it corresponds to a real profile and adjusted, if necessary, to satisfy this requirement. The base-profile shape corresponding to this adjusted velocity distribution is calculated. The airfoil velocity distribution is finally adjusted, if required, to take into account the modifications made to the original base-profile velocity distribution. The chordwise lift distribution is determined from this adjusted distribution. Then the chordwise lift distribution for the airfoil with the thickness removed is determined and the mean camber-line shape calculated. The calculated mean camber-line and base-profile shapes are then combined to give the airfoil section shape corresponding to the finally adjusted velocity distribution. In the example of the semi-low-drag airfoil, these steps are considered in detail.

Example I

(a) First choice

In general, a desired velocity distribution will be one laid out to some specified ideal lift coefficient, although it will only be required that the quarter-chord moment coefficient not be objectionably large. This, as will be seen later, allows the lift coefficient to be varied within a relatively large range without affecting the desired characteristics of the velocity distribution. Hence, under these conditions the ad-

justment to a particular ideal lift may be easily made after the base-profile-shape calculation is completed, provided the first choice of the velocity distribution is one having a lift coefficient within a few tenths of that desired.

In practically all cases it is required that the shape corresponding to some desired velocity distribution be one having a specified thickness ratio. This requirement—together with the requirement, discussed previously, that the desired velocity distribution corresponds to that for a real airfoil section which is both closed and pointed at the trailing edge—complicates the problem since it is not apparent from the velocity distribution whether these requirements are fulfilled. These complicating difficulties can and must largely be eliminated by choosing the velocity distribution wisely. Reference to known velocity distributions over existing airfoils having nearly the same thickness ratios and similar velocity distributions with that desired will aid in this choice.

Suppose, for example, that the semi-low-drag airfoil, used for illustration, is to have a low ideal lift coefficient and a maximum thickness equal to 14 percent of the chord, with an upper surface velocity distribution similar to that for a Joukowski base profile and a lower surface velocity distribution similar to that for an NACA 65-series low-drag base profile. It is to be expected under these conditions that reference to the velocity distribution over a Joukowski base profile for which  $t/c=0.14$ , and over an NACA 65-014 base profile will aid in the choice of the desired velocity distribution. In figure 14, the velocity distributions for these airfoils

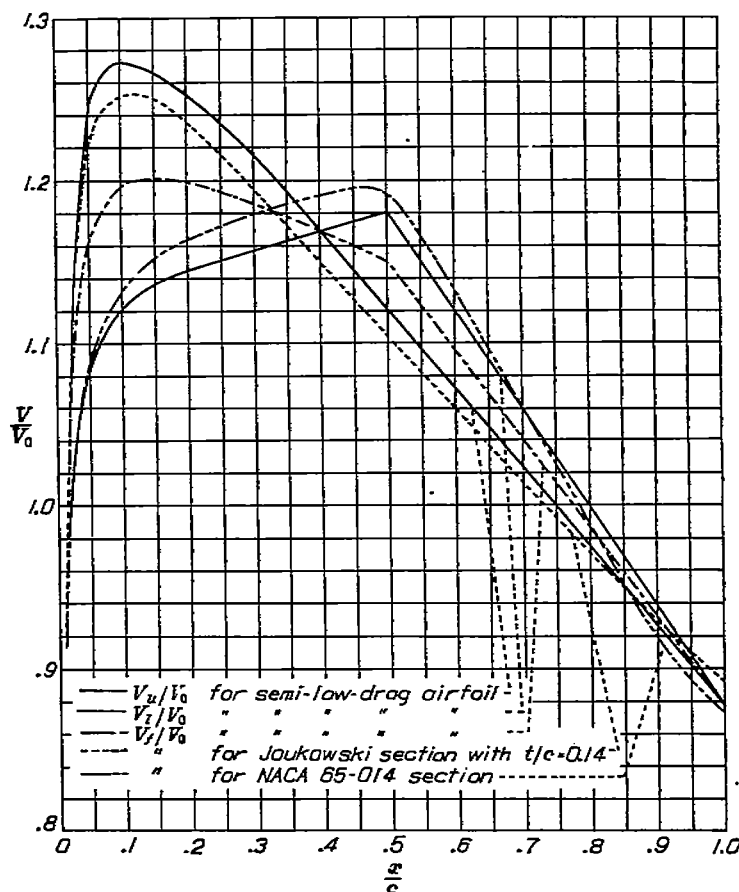


FIGURE 14.—Preliminary velocity distribution over the semi-low-drag airfoil.

are shown. The velocity distribution for the Joukowski section was taken directly from table II of this report. The NACA 65,2-016 is listed in reference 9, and the approximate velocity for the NACA 65-014, plotted in figure 14, was obtained using the approximate relation

$$\left(\frac{V_f}{V_0}\right)_{0.14} = 1 + \frac{0.14}{0.16} \left[ \left(\frac{V_f}{V_0}\right)_{0.16} - 1 \right]$$

Based on the foregoing consideration, a choice is made of the desired upper and lower surface velocity distributions, designated  $(V_u/V_0)_1$  and  $(V_l/V_0)_1$ , respectively, as in figure 14. The base-profile velocity distribution  $(V_f/V_0)_1$  shown in the figure is the average of these (loc. cit. equation (58)). The subscript 1 is used to denote that these velocity distributions are a "first trial."

Having decided upon the desired velocity distribution, the shape of the base profile is then determined as follows: A reference base profile which has nearly the same leading-edge radius as the airfoil to be derived is selected from the Joukowski base profiles listed in table II. The airfoil to be derived in the example will clearly have a leading-edge radius approximately midway between that for the Joukowski base profile, for which  $t/c=0.14$ , and the NACA 65-014. The leading-edge radius of the Joukowski base profile is

$$\frac{r_{L.E.}}{c} = 1.185 \left(\frac{t}{c}\right)^2 = 0.02322$$

For the NACA 65,2-016 from reference 9

$$\frac{r_{L.E.}}{c} = 0.01704$$

so for the NACA 65-014, since the leading-edge radius of any airfoil varies as the square of the thickness ratio,

$$\frac{r_{L.E.}}{c} = 0.01704 \left(\frac{0.14}{0.16}\right)^2 = 0.01305$$

The airfoil to be found will have approximately the leading-edge radius

$$\frac{r_{L.E.}}{c} = \frac{0.01305 + 0.02322}{2} = 0.0181$$

The Joukowski base profile for which  $t/c=0.12$  has nearly this radius (0.01706) and so is used as the reference profile in this example.

The difference between the desired and Joukowski base-profile velocity distributions is found from (table X)

$$\left(\frac{\Delta v}{V_0}\right)_1 = \left(\frac{V_f}{V_0}\right)_1 - \frac{V_f}{V_0} \quad (62)$$

and the values of  $(\Delta v/V_0)_1 \cos \theta$  are calculated using the values of the cosines given in the conversion table V. Then both  $(\Delta v/V_0)_1$  and  $(\Delta v/V_0)_1 \cos \theta$  are plotted as functions of  $\theta$  (fig. 15).

(b) Adjustment of first choice

In order that the desired velocity distribution will represent a real airfoil which closes and has a sharp trailing edge, it is required that the relations (loc. cit. equations (42))

$$\left. \begin{aligned} \int_0^\pi \frac{\Delta v}{V_0} d\theta &= 0 \\ \int_0^\pi \frac{\Delta v}{V_0} \cos \theta d\theta &= 0 \end{aligned} \right\} (63)$$

be satisfied.

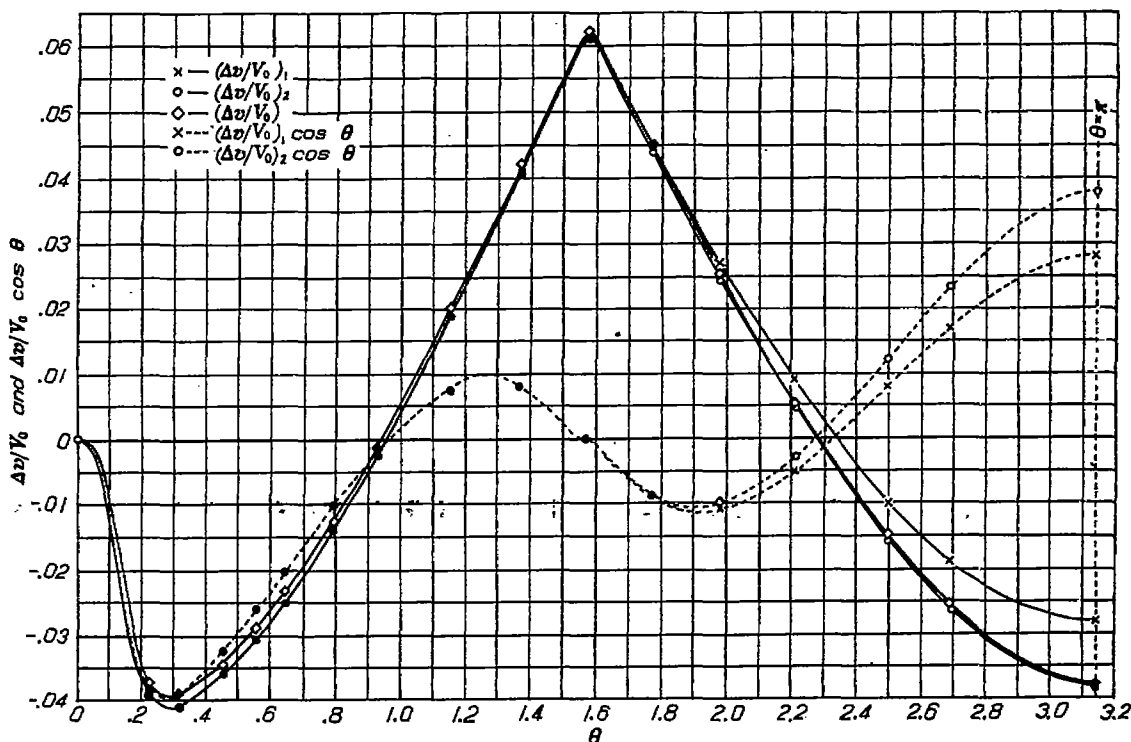


FIGURE 15.—Difference velocity distribution for semi-low-drag airfoil.

In the example, numerical integration of the curves of figure 15 gives

$$\int_0^\pi \left(\frac{\Delta v}{V_0}\right)_1 d\theta = +0.0046$$

$$\int_0^\pi \left(\frac{\Delta v}{V_0}\right)_1 \cos \theta d\theta = -0.0077$$

It is clear that if the values of  $(\Delta v/V_0)_1$  are decreased over the range  $\frac{1}{2}\pi < \theta < \pi$ , the integrals will both be nearer zero.

This suggests that as a second trial, the difference velocity distribution  $(\Delta v/V_0)_2$  shown in figure 15 will more nearly satisfy the integral equations (63) and at the same time will not destroy the desired characteristics of the given velocity distribution. In this case

$$\int_0^\pi \left(\frac{\Delta v}{V_0}\right)_2 d\theta = -0.0034$$

$$\int_0^\pi \left(\frac{\Delta v}{V_0}\right)_2 \cos \theta d\theta = -0.0012$$

The conditions of equations (63) are very nearly satisfied. The conditions may be satisfied completely by slightly translating and rotating the second trial of  $\Delta v/V_0$ . Assuming that a small increment

$$\Delta\left(\frac{\Delta v}{V_0}\right) = k_1 + k_2\left(\frac{\pi}{2} - \theta\right) \tag{64}$$

be added to the distribution  $(\Delta v/V_0)_2$ , since

$$\left. \begin{aligned} \int_0^\pi \Delta\left(\frac{\Delta v}{V_0}\right) d\theta &= \pi k_1 \\ \int_0^\pi \Delta\left(\frac{\Delta v}{V_0}\right) \cos \theta d\theta &= 2k_2 \end{aligned} \right\} \tag{65}$$

then making

$$k_1 = \frac{0.0034}{\pi} = 0.0011$$

and

$$k_2 = \frac{0.0012}{2} = 0.0006$$

the velocity distribution

$$\frac{\Delta v}{V_0} = \left(\frac{\Delta v}{V_0}\right)_2 + \Delta\left(\frac{\Delta v}{V_0}\right) \tag{66}$$

will completely satisfy the equations (63) as required.

In table X, the values of

$$\Delta\left(\frac{\Delta v}{V_0}\right) = 0.0011 + 0.0006\left(\frac{\pi}{2} - \theta\right)$$

are given and the difference velocity distribution  $\Delta v/V_0$  is calculated, using equation (66). These values are plotted as a function of  $\theta$  in figure 15. (The value at  $\theta=0$  is arbitrarily made zero.)

(c) Calculation of base-profile ordinates

The ordinates and slopes of the  $\Delta v/V_0$  curve at the proper  $\theta$  stations given in Appendix A for the numerical integration of equation (45) are found and listed, as in table XI. (Note that the value of the ordinate at station  $\pi + \theta$  is equal in sign and magnitude to the value at  $\pi - \theta$ .) The integration is performed, and the resulting values of  $d(\Delta y_t)/dx$  are plotted as functions of  $x/c$  (fig. 16) and integrated

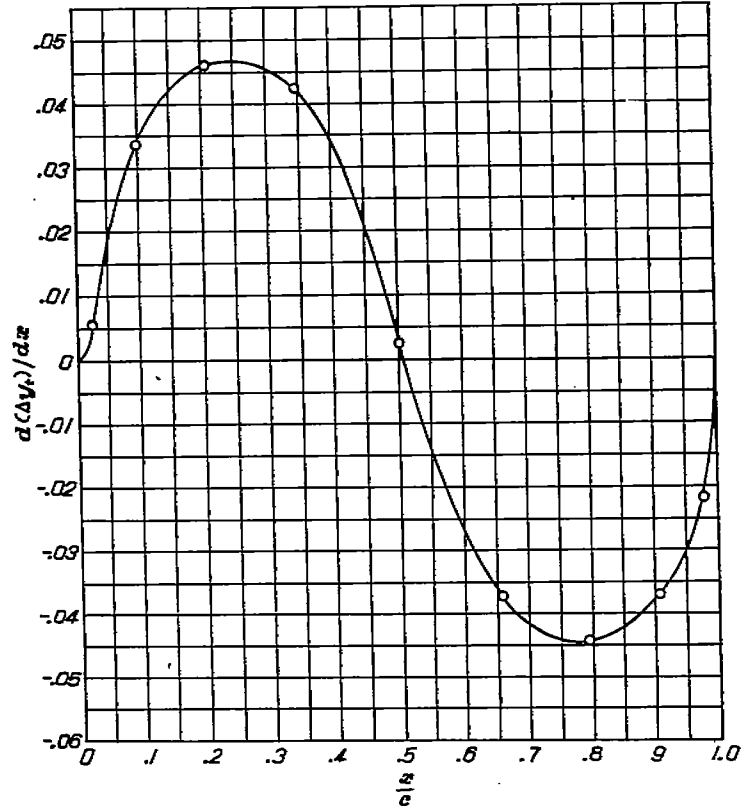


FIGURE 16.—Slope of the base profile ordinates for the semi-low-drag airfoil.

to give the values of  $\Delta y_t/c$  at the desired standard stations. The ordinates of the base profile are then found, as in table X, from

$$\frac{y_t}{c} = y_r + \frac{\Delta y_t}{c} \tag{67}$$

which corresponds to the velocity distribution

$$\frac{V_f}{V_0} = \frac{V_r}{V_0} + \left(\frac{\Delta v}{V_0}\right) \tag{68}$$

It is fortuitous that in this example the maximum thickness was precisely 14 percent of the chord as desired. In the event that the final thickness were  $t_1$  and that the desired thickness were  $t_2$ , the ordinates and velocity distribution, respectively, for the base profile of thickness  $t_2$  could be obtained from the equation

$$\left(\frac{y_t}{c}\right)_2 = \frac{t_2}{t_1} \left(\frac{y_t}{c}\right)_1 \tag{69}$$

and the approximate equation

$$\left(\frac{V_f}{V_0}\right)_2 = 1 + \frac{t_2}{t_1} \left[\left(\frac{V_f}{V_0}\right)_1 - 1\right] \tag{70}$$

## (d) Final adjustment

Before the calculation of the shape of the mean camber line corresponding to the given lift distribution is undertaken, it will be necessary to revise the lift distribution corresponding to the first trial of the given distribution so as to take into account the effect of the changes made to the original base-profile velocity distribution to make that velocity distribution represent a real profile. This may be done

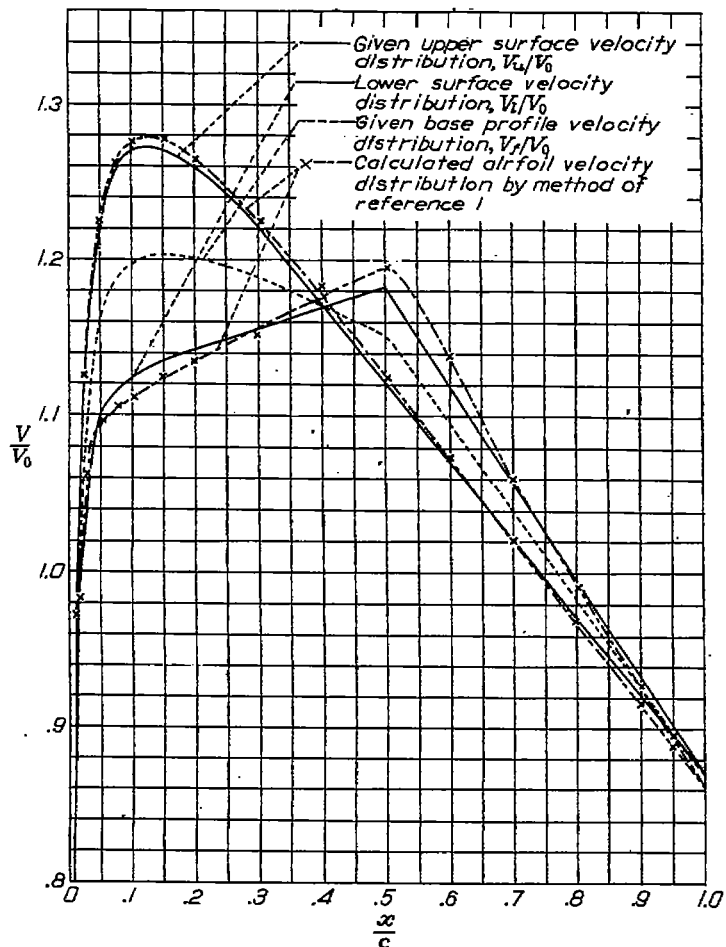


FIGURE 17.—Velocity distribution for semi-low-drag airfoil.

graphically on the plot of the corrected base-profile velocity distribution.

For example, in the case of the semi-low-drag airfoil used for illustration, the upper surface velocity distribution, to be similar to the Joukowski type of velocity distribution, must be nearly straight from the stations  $x/c=0.2$  to 1.0, as seen in figure 17. The base-profile velocity distribution must be a mean between the upper and lower surface velocity distributions; hence, when the upper surface distribution has been chosen, the lower surface distribution is determined

(fig. 17). The velocity distribution over the upper and lower surface of the leading-edge section ( $0 < x/c < 0.2$ ) is then suitably chosen so that the base-profile distribution is the mean. The basic chordwise lift distribution is related to the upper and lower surface velocity distributions by (loc. cit. equations (58)).

$$\left. \begin{aligned} \frac{V_u}{V_0} &= \frac{V_f}{V_0} + \frac{P_b/4}{V_f/V_0} \\ \frac{V_l}{V_0} &= \frac{V_f}{V_0} - \frac{P_b/4}{V_f/V_0} \end{aligned} \right\} \quad (71)$$

## (e) Calculation of mean camber-line ordinates

Now in the calculation of the mean camber-line shape (table XII), the basic lift distribution corresponding to zero profile thickness  ${}_0P_b$  must be used. From equation (54)

$${}_0P_b = \frac{P_b}{V_f/V_0} \quad (72)$$

so that this distribution can be obtained directly from

$${}_0P_b = 2 \left( \frac{V_u}{V_0} - \frac{V_l}{V_0} \right) \quad (73)$$

To determine the mean camber-line shape which will promote this lift distribution, the procedure is as follows: The value of  ${}_0P_b/4$  is plotted as a function of  $\theta$  (fig. 18). The ordinates and slopes at the proper  $\theta$  stations given in Appendix A for the numerical integration of equation (27) are found (table XIII) and the integration performed. (Note that the value of  ${}_0P_b/4$  at station  $\pi+\theta$  is equal in magnitude but opposite in sign to that at  $\pi-\theta$ ). The resulting values of  $dy_{cb}/dx$  are plotted as a function of  $x/c$  (fig. 19) and the values of  $y_{cb}$  obtained by integration.

The resulting mean camber line is at the ideal angle of attack (the angle of attack for which the additional lift distribution is zero) and hence, unless the ideal angle is zero, the trailing edge is either below or above the  $x/c$  axis. Ordinates of camber lines are generally specified with the extremities of the camber line on the  $x/c$  axis and designated by the conventional symbol  $y_c$ .

The ideal angle of attack is simply

$$\alpha_i = \left( \frac{y_{cb}}{c} \right)_{x/c=0} - \left( \frac{y_{cb}}{c} \right)_{x/c=1.0} \quad (74)$$

and

$$\left. \begin{aligned} \frac{y_c}{c} &= \frac{y_{cb}}{c} + \frac{x}{c} \alpha_i \\ \frac{dy_c}{dx} &= \frac{dy_{cb}}{dx} + \alpha_i \end{aligned} \right\} \quad (75)$$

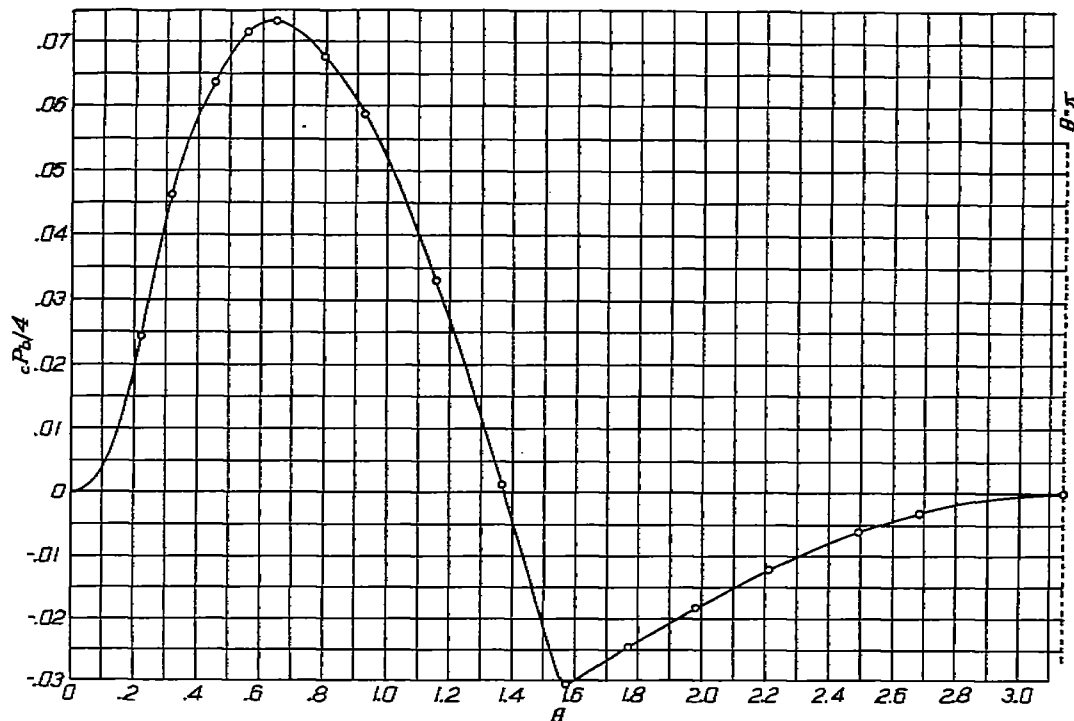


FIGURE 18.—Quarter base lift distribution,  $cP_n/4$  for semi-low-drag airfoil.

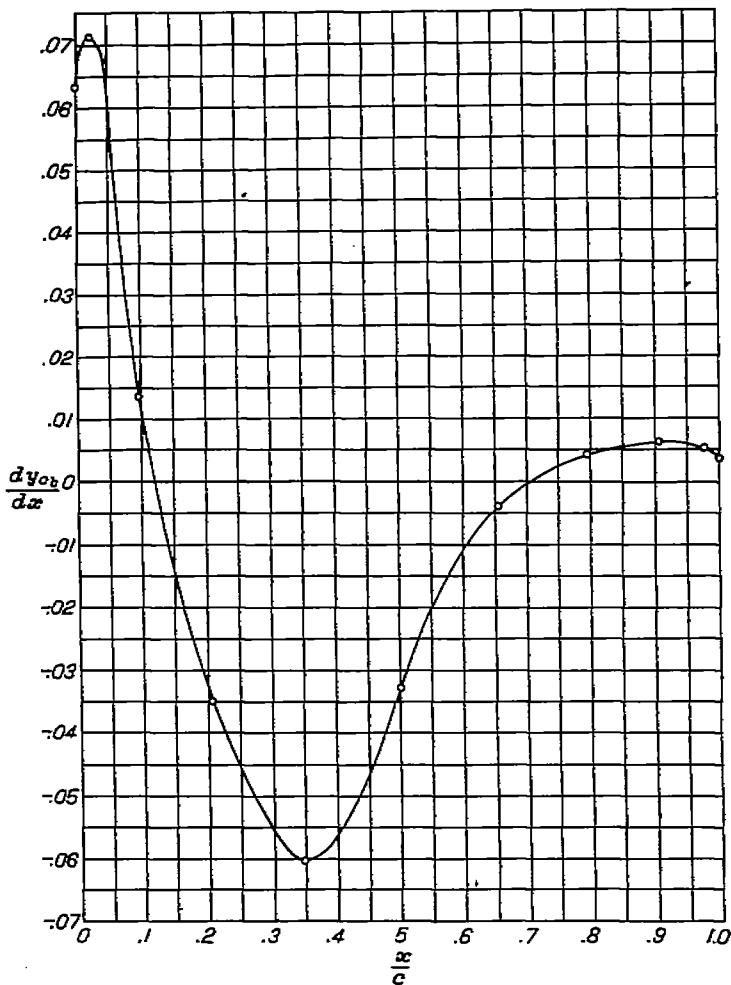


FIGURE 19.—Slopes of the mean camber line ordinates for the semi-low-drag airfoil.

In the case of the semi-low-drag airfoil used for the example

$$\alpha_i = +0.01233 \text{ radians} = 0.706^\circ$$

and the values of  $y_c/c$  and  $dy_c/dx$  listed in table XII are obtained from the equations

$$\frac{y_c}{c} = \frac{y_{c_0}}{c} + 0.01233 \frac{x}{c}$$

$$\frac{dy_c}{dx} = \frac{dy_{c_0}}{dx} + 0.01233$$

Using these values of  $y_c/c$  and  $dy_c/dx$  along with the previously determined values of  $y_i/c$ , the ordinates of the airfoil can be calculated, as shown in table XIV for the semi-low-drag airfoil used as an example, from

$$\left. \begin{aligned} \frac{x_u}{c} &= \frac{x}{c} - \frac{y_i}{c} \sin \beta \\ \frac{y_u}{c} &= \frac{y_c}{c} + \frac{y_i}{c} \cos \beta \\ \frac{x_i}{c} &= \frac{x}{c} + \frac{y_i}{c} \sin \beta \\ \frac{y_i}{c} &= \frac{y_c}{c} - \frac{y_i}{c} \cos \beta \end{aligned} \right\} \quad (76)$$

where

$$\beta = \tan^{-1} \left( \frac{dy_c}{dx} \right)$$

The resulting airfoil is shown in figure 20.

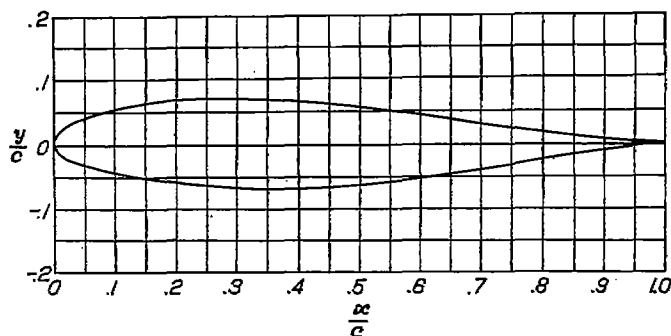


FIGURE 20.—Semi-low-drag airfoil.

The chordwise basic lift distribution over the airfoil is found from

$$P_b = {}_0P_b \left( \frac{V_f}{V_0} \right) \quad (77)$$

and is plotted and integrated to give the basic (or ideal) lift coefficient. For this semi-low-drag airfoil, the basic lift distribution was plotted and the value of the basic lift coefficient was found by integration to be

$$c_{l_b} = 0.0489$$

The velocity distribution over this semi-low-drag airfoil was calculated by the method of reference 1 at this value of the lift coefficient. The results of this calculation are shown in figure 17 to an enlarged scale of  $V/V_0$  for comparison with the given (solid line) distribution. It is seen that the agreement is close.

If it is desired to calculate the velocity distribution at a value of the lift coefficient other than the basic lift coefficient, the procedure to be followed is that given under the heading entitled Applications of the Method.

In the preceding analysis it was tacitly assumed that the lift and quarter-chord moment coefficients corresponding to the finally adjusted velocity distribution were those desired. It is clear that in the final adjustment these coefficients could have been adjusted by changing the upper and lower velocity distributions, taking care only to keep the average of these equal to the base-profile velocity distribution. On the other hand, since superposition of camber lines is always permissible, such adjustments can be made at any time. There are, of course, an infinite number of adjustments possible, some of which are particularly convenient. As an example, the  $a=1$  type mean camber line (reference 9) can be conveniently used to adjust the lift or quarter-chord moment coefficient of this semi-low-drag airfoil. Since the addition of this camber line simply shifts the upper and lower surface velocity distributions up or down with respect to that of the base profile, these adjustments do not disturb the desired characteristics of the velocity distribution.

To cite one example, suppose it is desired that the semi-low-drag airfoil be adjusted to an ideal lift coefficient of 0.4. With this base profile the  $a=1$  type mean camber line for  ${}_0c_{l_b}$  of unity attains a lift coefficient  $c_{l_b} = 1.080$  (loc. cit.

equation (29)). The required lift coefficient for this component of the basic lift is

$$0.4000 - 0.0489 = 0.3511$$

so that if the mean camber-line ordinates of the  $a=1$  type for  ${}_0c_{l_b}$  of unity given in reference 9 are multiplied by

$$\frac{0.3511}{1.080} = 0.325$$

and the resulting ordinates added to those in table XII, a new mean camber line for which  $c_{l_b} = 0.4$  is obtained. These in turn can be combined with the original ordinates of the base profile to give the corresponding airfoil ordinates.

As a second example, suppose it is desired that the semi-low-drag airfoil be adjusted to zero quarter-chord-moment coefficient. For the mean camber line given in table XII, the quarter-chord-moment coefficient is  $+0.0224$ . The  $a=1$  type mean camber line for  ${}_0c_{l_b}$  of unity attains a quarter-chord-moment coefficient of  $-0.2506$ , or, for  $c_{m_{c/4}} = -0.0224$  the corresponding  ${}_0c_{l_b} = 0.0894$  and  $c_{l_b} = 0.0965$ . Hence, zero quarter-chord-moment coefficient can be obtained by combining the original mean camber line with an  $a=1$  type camber line for which  ${}_0c_{l_b} = 0.0894$ . The corresponding basic lift coefficient is

$$c_{l_b} = 0.0489 + 0.0965 = 0.1454$$

In retrospect, it can be seen that the more exacting the characteristics of the desired velocity distribution, the more attention must be given to the first choice and final adjustment of this distribution. In the case of the semi-low-drag airfoil used for illustration, it should be quite clear that had the desired lift and moment characteristics both been specified, the effort required to obtain a satisfactory first choice and final adjusted velocity distribution would be considerably increased. The possible variations in the choice of desired velocity distributions are unlimited so that no general rules can be laid down for the special treatment required in each and every case. Facility in the use of this method for the inverse problem can be acquired only through experience.

#### Example II

Experimental studies of a large number of low-drag airfoils have been made in which the effects of various modifications in pressure distribution were determined. Airfoils having pressure-distribution characteristics like that of the series 3 and 6 low-drag airfoils were found to be definitely superior in most respects. The somewhat decreasing but nearly constant favorable pressure gradients which occur over the forward part of such airfoils, from the nose section—where severe gradients due to the necessary rounded leading edge occur—to the minimum pressure point, are desirable. This allows relatively large additional lift increments to be added, as well as some waviness of surface to be tolerated, without such additional lift or waviness promoting local adverse pressure gradients and so “premature” transition to turbulent flow in the favorable gradient region. The

nearly constant adverse gradient back of minimum pressure has been found to be influential in increasing the critical boundary-layer Reynolds number at the transition point with given surface conditions, and so increasing the upper limit of the Reynolds number range for lowest drag coefficients.

Airfoils similar to the NACA series 3, 4, and 6 low-drag airfoils are obtained by superposing the ordinates of a base-profile shape which promotes a double-roof form of velocity distribution on the ordinates of an appropriate Joukowski base profile. The problem of finding the shape corresponding to the double-roof velocity distribution, although it was solved originally for the NACA series 3 low-drag airfoils and series 4 high-critical-compressibility-speed airfoils by use of the numerical method (equation (45)), is a rather important example of one which may be solved by integration using the trigonometric expressions for the velocity distribution in equation (43). In trigonometric form, the equations for the double-roof velocity distribution are

$$\left. \begin{aligned} \frac{\Delta v}{V_0} &= k_1 + k_2 \cos \theta & 0 < \theta < \theta_m \\ \frac{\Delta v}{V_0} &= k_3 + k_4 \cos \theta & \theta_m < \theta < \pi \end{aligned} \right\} \quad (78)$$

where  $\theta$  corresponds the point  $x$  and  $\theta_m$  corresponds to the minimum pressure point  $x_m$ .

The conditions that the value of  $\Delta v/V_0$  must be the same in either equation at  $\theta_m$  and that the equations (42) be satisfied require that

$$\left. \begin{aligned} k_1 &= \frac{s}{2} \left[ \frac{\sin \theta_m + (\pi - \theta_m) \cos \theta_m}{\cos \theta_m \sin \theta_m + \pi - \theta_m} \right] \\ k_2 &= -\frac{s}{2} \\ k_3 &= \frac{s}{2} \left[ \frac{\sin \theta_m - \theta_m \cos \theta_m}{\cos \theta_m \sin \theta_m + \pi - \theta_m} \right] \\ k_4 &= -\frac{s}{2} \left[ \frac{\cos \theta_m \sin \theta_m - \theta_m}{\cos \theta_m \sin \theta_m + \pi - \theta_m} \right] \end{aligned} \right\} \quad (79)$$

where  $s$  is the slope of the velocity curve between  $x/c=0$  and  $x/c=x_m/c$ ; that is,

$$s = \frac{\left(\frac{\Delta v}{V_0}\right)_{x/c=x_m/c} - \left(\frac{\Delta v}{V_0}\right)_{x/c=0}}{x_m/c} \quad (80)$$

The corresponding shape of the base profile which will promote this velocity distribution is

$$\frac{\Delta y}{c} = \frac{s}{8} \left[ \frac{\sin \theta_m \sin \theta (1 - \cos \theta \cos \theta_m) - (\cos \theta_m - \cos \theta)^2 \ln \left| \frac{\sin \frac{1}{2}(\theta_m + \theta)}{\sin \frac{1}{2}(\theta_m - \theta)} \right|}{\cos \theta_m \sin \theta_m + \pi - \theta_m} \right] \quad (81)$$

where the vertical bars indicate the absolute value. In table XV, the velocity distribution and ordinates of the double-roof base profile which may be superimposed on other base profiles are given.

For those double-roof base profiles the value of  $\Delta v/V_0$  is not zero at  $x=0$ , so that it is obviously incorrect to superpose such base profiles on a reference base profile having an infinite slope at the leading edge since for such reference base profiles  $V_r/V_0=0$ . Nevertheless, the velocity distribution calculated by superposition for such combined profiles is in reasonably satisfactory agreement with experiment except in the immediate vicinity of the leading edge.

By combining these double-roof base profiles with a suitable reference base profile, a variety of satisfactory low-drag airfoils can be derived. An example is the superposition of a double-roof base profile for which  $x_m=0.4c$  and  $s_{0.4}=0.3059$ , and a double-roof base profile in which  $x_m=0.7c$  and  $s_{0.7}=0.1367$  (table XV) on a Joukowski base profile for which  $t/c=0.10$  (table II). A base profile results which, when combined with a type  $a=0.4$ ,  $c_b=0.8201$  mean camber line superposed on a type  $a=0.7$ ,  $c_b=-0.5513$  mean camber line gives an airfoil for which  $t/c=0.14$  and which has an upper-surface velocity distribution similar in form to that of the NACA 64-series low-drag airfoil and a lower-surface velocity distribution similar in form to the NACA 67-series low-drag airfoil. This airfoil, the velocity distribution for which is shown to an expanded scale of  $V/V_0$  by the solid-line curve in figure 21, is completely satis-

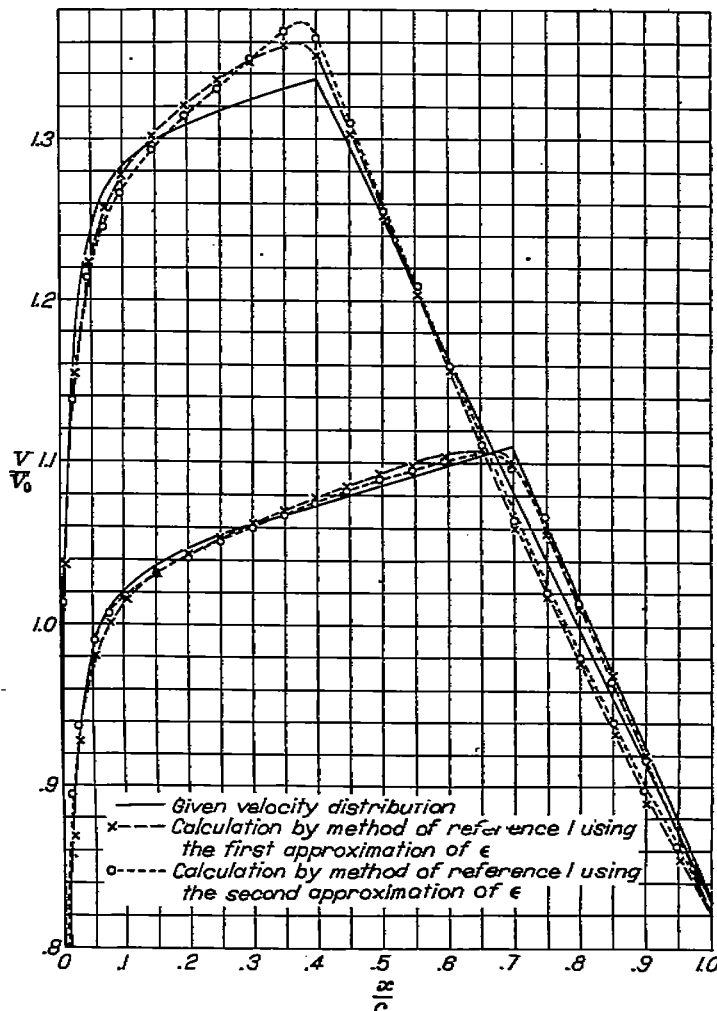


FIGURE 21.—Velocity distribution over a low-drag airfoil having minimum pressure at 0.4c on upper surface and 0.7c on lower surface.

factory except for the fact that the nose radius is unnecessarily small so that the maximum lift coefficient may be adversely affected. One way in which this difficulty may be alleviated to some extent is to add the increment  $\Delta y_t$  normal to the surface of the reference base profile rather than normal to the  $x$ -axis so that the ordinates are given by

$$y_t = y_r + \Delta y_t \sqrt{1 + \left(\frac{dy_r}{dx}\right)^2} \quad (82)$$

where  $dy_r/dx$  is the slope of the surface of the reference base profile at the station under consideration. This procedure is hardly justifiable, however.

A very satisfactory method for improving the shape at the leading edge is to calculate the velocity distribution over the base profile carefully by the method of reference 1. Then, by using the graphical method of reference 12, a change in shape of the base profile and the corresponding change in the velocity distribution may be found by trial which will allow an increase in the leading-edge radius that will not promote a "bump" in the velocity distribution near the leading edge.

#### DISCUSSION AND CONCLUSIONS

In the theoretical development of the method of this report a number of simplifying assumptions were made in order to facilitate the mathematical treatment, some of which are clearly contrary to fact. The method of reference 1 by comparison would appear exact. However, two assumptions common to the development of both methods are that the fluid is incompressible and nonviscous. The first is justifiable if the velocities are everywhere negligibly small in comparison with the velocity of sound. The second can never be considered strictly justifiable although in the usual Reynolds number range the error is small. It should be noted, however, that in the usual case, as may be seen in figure 12, the inaccuracy of the method of this report resulting from all the other assumptions except that concerning the viscosity of the fluid (and compressibility when it is important) is small as compared with the inaccuracies of both methods resulting from the neglect of the effects of viscosity (and compressibility).

Concerning the method of reference 1, it has been found that the second approximation for the value of  $\epsilon$  should be employed in the calculation if the base profile under consideration differs markedly from the Joukowski base profile,

as is the case with a number of low-drag airfoils, particularly for thick sections or for those sections with the minimum pressure point far back along the chord. The inadequacy of the first approximation is not very evident in figure 21, wherein the velocity distribution as calculated by the method of reference 1 using both the first and second approximations is shown for comparison with the method of this report, since the maximum thickness is fairly far forward and the airfoil is relatively thin.

The satisfactory application of the methods of this report rests on a thorough understanding of the limitations on the principle of superposition as it applies to the mean camber line and the base profile. In the theory of the mean camber line it was assumed that the camber, as well as the slope of the camber line, was small. Hence, superposition of mean camber lines or of lift distributions should be permissible for all usual camber lines, provided the camber or lift is small. Experiment has shown that for usual mean camber lines calculations based on this method are in good agreement with experiment, provided the basic lift coefficient is less than unity, but that even up to basic lift coefficients of two the agreement is fair. In the theory of the base profile it was assumed, in effect, that the slope of the surface is small. At the leading edge of an airfoil section and at the leading and trailing edges of a strut section, the slope of the profile is infinite so that, as was shown for the Joukowski and elliptic base profiles, the method of this report cannot be used directly to determine the velocity distribution or shape of such bodies. Rather, the method must be used to determine the change in velocity distribution or shape corresponding to some specified change in shape or velocity distribution, respectively. This change can represent a marked alteration in shape at all points except the leading and trailing edges.

Again, in the theory of the base profile, it was assumed that the profile is thin. Experiments have indicated that the method is satisfactory for all airfoils of usual thickness (up to thickness-chord ratios of 0.18) and even reasonably satisfactory in the case of an airfoil having a thickness-chord ratio of 0.25 (NACA 45-125).

AMES AERONAUTICAL LABORATORY,  
NATIONAL ADVISORY COMMITTEE FOR AERONAUTICS,  
MOFFETT FIELD, CALIF.

## APPENDIX A

### NUMERICAL INTEGRATION METHODS

A numerical evaluation of the integral

$$E = \frac{1}{2\pi} \int_0^{2\pi} F \cot \frac{\theta - \theta_0}{2} d\theta$$

is given in the appendix of reference 1.

A "20-point" solution is

$$E = a_0 \left( \frac{dF}{d\theta} \right)_0 + a_1(F_1 - F_{-1}) + a_2(F_2 - F_{-2}) + \dots + a_9(F_9 - F_{-9})$$

where  $F_1$  is the value of  $F$  at  $\theta_0 + \frac{\pi}{10}$

$F_n$  is the value of  $F$  at  $\theta_0 + \frac{n\pi}{10}$

( $n=1, -1, 2, -2, \dots, 9, -9$ )

$\left( \frac{dF}{d\theta} \right)_0$  is the value of  $\left( \frac{dF}{d\theta} \right)$  at  $\theta = \theta_0$

and the coefficients are

$a_0 = 0.1000$	$a_5 = 0.0503$
$a_1 = 0.3473$	$a_6 = 0.0366$
$a_2 = 0.1572$	$a_7 = 0.0281$
$a_3 = 0.0996$	$a_8 = 0.0163$
$a_4 = 0.0691$	$a_9 = 0.0080$

The value of  $\Delta v/V_0$  for  $\theta = 4\pi/10$  given in table IV for the NACA 4412 base profile, for example, is obtained in the following cyclic form:

$$\frac{\Delta v}{V_0} = - \left[ \begin{array}{l} 0.1000(+0.0138) \\ +0.3473(+0.0283-0.0192) \\ +0.1572(+0.0178-0.0006) \\ +0.0996(-0.0044+0.0397) \\ +0.0691(-0.0406+0) \\ +0.0503(-0.0901-0.0397) \\ +0.0366(0+0.0006) \\ +0.0281(+0.0901+0.0192) \\ +0.0163(+0.0406+0.0283) \\ +0.0080(+0.0044+0.0283) \end{array} \right] = -0.0059$$

A more accurate "40-point" solution is

$$E = b_0 \left( \frac{dF}{d\theta} \right)_0 + b_1(F_1 - F_{-1}) + b_2(F_2 - F_{-2}) + \dots + b_{19}(F_{19} - F_{-19})$$

where now

$F_1$  is the value of  $F$  at  $\theta_0 + \frac{\pi}{20}$

$F_n$  is the value of  $F$  at  $\theta_0 + \frac{n\pi}{20}$

( $n=1, -1, 2, -2, \dots, 19, -19$ )

$\left( \frac{dF}{d\theta} \right)_0$  is the value of  $\frac{dF}{d\theta}$  at  $\theta = \theta_0$

and the coefficients are given by

$b_0 = 0.05000$	$b_{10} = 0.02503$
$b_1 = 0.34906$	$b_{11} = 0.02139$
$b_2 = 0.16129$	$b_{12} = 0.01819$
$b_3 = 0.10514$	$b_{13} = 0.01532$
$b_4 = 0.07735$	$b_{14} = 0.01273$
$b_5 = 0.06057$	$b_{15} = 0.01036$
$b_6 = 0.04918$	$b_{16} = 0.00814$
$b_7 = 0.04087$	$b_{17} = 0.00599$
$b_8 = 0.03444$	$b_{18} = 0.00395$
$b_9 = 0.02929$	$b_{19} = 0.00197$

The 40-point solution need be employed only when the function  $F$  changes more or less abruptly with  $x/c$ .

### REFERENCES

1. Theodorsen, T., and Garrick, I. E.: General Potential Theory of Arbitrary Wing Sections. NACA Rep. No. 452, 1933.
2. Theodorsen, Theodore: Theory of Wing Sections of Arbitrary Shape. NACA Rep. No. 411, 1931.
3. Betz, A.: Modification of Wing-Section Shape to Assure a Predetermined Change in Pressure Distribution. NACA TM No. 767, 1935.
4. Allen, H. Julian: A Simplified Method for the Calculation of Airfoil Pressure Distribution. NACA TN No. 708, 1939.
5. Glauert, H.: The Elements of Aerofoil and Airscrew Theory. The University Press (Cambridge), 1926, pp. 87-93.
6. Theodorsen, Theodore: On the Theory of Wing Sections with Particular Reference to the Lift Distribution. NACA Rep. No. 383, 1931.
7. Jacobs, Eastman N., and Rhode, R. V.: Airfoil Section Characteristics as Applied to the Prediction of Air Forces and Their Distribution on Wings. NACA Rep. No. 631, 1938.
8. Allen, H. Julian: Calculation of the Chordwise Load Distribution over Airfoil Sections with Plain, Split, or Specially Hinged Trailing-Edge Flaps. NACA Rep. No. 634, 1938.
9. Abbott, Ira H., von Doenhoff, Albert E., and Stivers, Louis S., Jr.: Summary of Airfoil Data. NACA Rep. No. 824, 1945.
10. Jacobs, Eastman N., Ward, Kenneth E., and Pinkerton, Robert M.: The Characteristics of 78 Related Airfoil Sections from Tests in the Variable-Density Wind Tunnel. NACA Rep. No. 460, 1933.
11. Pinkerton, Robert M.: Calculated and Measured Pressure Distributions over the Midspan Section of the N. A. C. A. 4412 Airfoil. NACA Rep. No. 563, 1936.
12. Jones, Robert T., and Cohen, Doris: A Graphical Method of Determining Pressure Distribution in Two-Dimensional Flow. NACA Rep. No. 722, 1941.

TABLE I.—CALCULATED VALUES OF ADDITIONAL LIFT COEFFICIENT DISTRIBUTION  $\frac{\Delta P_a}{\rho c l_a}$  FOR INFINITELY THIN AIRFOILS

$$\frac{\Delta P_a}{\rho c l_a} = \frac{2(1 + \cos \theta)}{\pi \sin \theta} = \frac{2}{\pi} \sqrt{\frac{1-x/c}{x/c}}$$

$\frac{x}{c}$	$\frac{\Delta P_a}{\rho c l_a}$	$\frac{x}{c}$	$\frac{\Delta P_a}{\rho c l_a}$
0	$\infty$	.4500	.704
.0125	5.658	.5000	.637
.0250	3.976	.5500	.576
.0500	2.775	.6000	.520
.0750	2.235	.6500	.467
.1000	1.910	.7000	.417
.1500	1.515	.7500	.368
.2000	1.273	.8000	.318
.2500	1.103	.8500	.267
.3000	.973	.9000	.212
.3500	.868	.9500	.146
.4000	.780	1.0000	0

TABLE II.—SURFACE ORDINATES AND VELOCITIES FOR JOUKOWSKI BASE PROFILES

$\frac{x}{c}$	$t/c=0.02$		$t/c=0.04$		$t/c=0.06$		$t/c=0.08$		$t/c=0.10$		$t/c=0.12$		$t/c=0.14$	
	$y/c$	$V_r/V_0$												
0	0	0	0	0	0	0	0	0	0	0	0	0	0	0
.005	.0021808	1.0230	.0043170	1.0045	.0064662	0.9889	.0086040	0.9016	.0107236	0.8427	.0128292	0.7875	.0149061	0.7379
.0075	.0026358	1.0306	.0052674	1.0321	.0078900	1.0107	.0104992	0.9749	.0130910	.9322	.0156613	0.8579	.0182067	0.8449
.0125	.0033772	1.0367	.0067491	1.0556	.0101096	1.0583	.0134536	1.0479	.0167757	1.0262	.0200710	1.0026	.0233361	0.9733
.025	.0040858	1.0407	.0093647	1.0782	.0140288	1.0971	.0180712	1.1128	.0232853	1.1210	.0278644	1.1226	.0324027	1.1190
.05	.0063737	1.0416	.0127393	1.0799	.0190873	1.1145	.0254096	1.1452	.0316982	1.1719	.0379454	1.1946	.0441435	1.2132
.075	.0075003	1.0408	.0149925	1.0789	.0224669	1.1171	.0291184	1.1522	.0373298	1.1849	.0447022	1.2151	.0530252	1.2428
.10	.0083121	1.0396	.0166168	1.0783	.0249050	1.1159	.0311690	1.1524	.0414012	1.1872	.0495942	1.2206	.0577410	1.2624
.15	.0098443	1.0308	.0186836	1.0736	.0280109	1.1096	.0337820	1.1454	.0460080	1.1807	.0568069	1.2154	.0650827	1.2495
.20	.0098625	1.0338	.0197030	1.0676	.0295472	1.1014	.0363826	1.1350	.0492067	1.1686	.0630107	1.2019	.0698103	1.2351
.25	.0099996	1.0308	.0200000	1.0616	.0300000	1.0924	.0400002	1.1233	.0500000	1.1542	.0600015	1.1851	.0700034	1.2161
.30	.0098778	1.0277	.0197585	1.0554	.0298445	1.0832	.0395986	1.1110	.0494436	1.1368	.0593626	1.1608	.0692958	1.1949
.35	.0095466	1.0246	.0190994	1.0492	.0286614	1.0737	.0382253	1.0983	.0478351	1.1230	.0583525	1.1478	.0679034	1.1727
.40	.0090516	1.0215	.0181107	1.0429	.0271825	1.0643	.0362743	1.0856	.0453930	1.1070	.0548239	1.1284	.0637395	1.1500
.45	.0084262	1.0184	.0168610	1.0366	.0253107	1.0545	.0337838	1.0723	.0422853	1.0909	.0509326	1.1090	.0594254	1.1271
.50	.0076991	1.0163	.0154070	1.0304	.0231811	1.0453	.0308902	1.0601	.0386631	1.0748	.0464857	1.0890	.0543565	1.1043
.55	.0068946	1.0122	.0137680	1.0241	.0207177	1.0359	.0273624	1.0474	.0346412	1.0589	.0416628	1.0702	.0497372	1.0816
.60	.0060350	1.0091	.0120784	1.0179	.0181372	1.0265	.0242199	1.0345	.0303348	1.0430	.0364906	1.0511	.0426365	1.0590
.65	.0051413	1.0060	.0102902	1.0117	.0154829	1.0171	.0206871	1.0223	.0258503	1.0273	.0311093	1.0322	.0363956	1.0363
.70	.0042340	1.0029	.0084744	1.0055	.0127269	1.0079	.0166970	1.0100	.0212920	1.0118	.0256134	1.0136	.0293933	1.0150
.75	.0033340	.9998	.0066730	.9994	.0100214	.9987	.0133844	.9977	.0167670	.9965	.0201745	.9951	.0236127	.9934
.80	.0024658	.9968	.0049314	.9933	.0074058	.9936	.0098908	.9938	.0123902	.9914	.0149079	.9909	.0174490	.9907
.85	.0016495	.9937	.0033015	.9872	.0049679	.9905	.0066212	.9936	.0082938	.9964	.0099774	.9991	.0116776	.9916
.90	.0009239	.9907	.0018491	.9812	.0027767	.9715	.0037079	.9817	.0046441	.9817	.0053806	.9816	.0063368	.9813
.95	.0003358	.9876	.0006716	.9752	.0010085	.9626	.0019465	.9500	.0010862	.9432	.0020290	.9243	.0023728	.9114
1.00	0	.9845	0	.9692	0	.9536	0	.9384	0	.9229	0	.9072	0	.8919
	$\frac{T.L.E.}{c} = -0.00047$		$\frac{T.L.E.}{c} = -0.00190$		$\frac{T.L.E.}{c} = -0.00427$		$\frac{T.L.E.}{c} = -0.00758$		$\frac{T.L.E.}{c} = -0.01185$		$\frac{T.L.E.}{c} = -0.01706$		$\frac{T.L.E.}{c} = -0.02323$	

TABLE III.—BASE-PROFILE VELOCITY-DISTRIBUTION CALCULATION FOR NACA 4412 AIRFOIL SECTION

$\frac{x}{c}$	$\frac{y}{c}$	$\frac{y_r}{c}$	$\frac{\Delta y_r}{c}$	$\frac{d(\Delta y_r)}{dx}$	$\theta$	$\frac{V_r}{V_0}$	$\frac{\Delta P}{V_0}$	$\frac{V_r}{V_0}$
0	0	0	0	0	0	0	0	0
.0125	.01894	.02007	-.00113	-.0612	.2241	1.003	-.016	.987
.025	.02615	.02780	-.00171	-.0382	.3176	1.123	-.024	1.099
.05	.03555	.03795	-.00240	-.0182	.4510	1.195	-.032	1.163
.075	.04200	.04470	-.00270	-.0070	.5548	1.215	-.034	1.181
.1	.04653	.04989	-.00336	-.0012	.6436	1.231	-.033	1.188
.15	.05345	.05687	-.00342	.0122	.7054	1.218	-.028	1.187
.2	.05738	.05902	-.00164	.0185	.7273	1.202	-.023	1.179
.25	.05941	.06000	-.00059	.0224	1.0472	1.186	-.017	1.168
.3	.06002	.06036	-.00036	.0266	1.1893	1.187	-.011	1.166
.4	.05803	.05462	.00361	.0230	1.3604	1.128	.001	1.129
.5	.05294	.04649	.00645	.0280	1.5708	1.090	.013	1.103
.6	.04563	.03649	.00914	.0253	1.7722	1.051	.025	1.076
.7	.03064	.02562	.00502	.0102	1.9823	1.014	.036	1.050
.8	.02823	.01491	.01332	-.0053	2.2143	.977	.045	1.022
.9	.01448	.00559	.00889	-.0410	2.4981	.942	.040	.982
.95	.00907	.00203	.00704	-.0685	2.6906	.924	.018	.942
1.00	.00126	0	.00126	-----	3.1416	-----	-----	-----

TABLE IV.—INTEGRATION CALCULATION OF  $\Delta P/V_0$  FOR NACA 4412 BASE PROFILE

$\theta$	$\frac{d(\Delta y_r)}{dx}$	$\frac{d}{d\theta} \left[ \frac{d(\Delta y_r)}{dx} \right]$	$\frac{\Delta P}{V_0}$	$\frac{x}{c}$
0	0	0	-----	0
$\pi/10$	-.0397	.1875	-.0226	.0214
$2\pi/10$	-.0006	.0867	-.0332	.0553
$3\pi/10$	.0192	.0423	-.0219	.0661
$4\pi/10$	.0283	.0193	-.0059	.0458
$5\pi/10$	.0283	-.0140	.0129	.0000
$6\pi/10$	.0178	-.0523	.0317	.0546
$7\pi/10$	-.0044	-.0938	.0443	.0699
$8\pi/10$	-.0406	-.1255	.0101	.0845
$9\pi/10$	-.0901	-.1837	-.0061	.0756
$\pi$	0	0	-----	1.0000
$11\pi/10$	.0901	-----	-----	-----
$12\pi/10$	.0406	-----	-----	-----
$13\pi/10$	.0044	-----	-----	-----
$14\pi/10$	-.0178	-----	-----	-----
$15\pi/10$	-.0283	-----	-----	-----
$16\pi/10$	-.0283	-----	-----	-----
$17\pi/10$	-.0192	-----	-----	-----
$18\pi/10$	-.0006	-----	-----	-----
$19\pi/10$	.0397	-----	-----	-----
$2\pi$	0	-----	-----	-----

TABLE V.—COORDINATE CONVERSION TABLE

$\frac{x}{c}$	$\cos \theta$	$\sin \theta$	$\theta$ (radians)	$\theta$ (radians)	$\cos \theta$	$\sin \theta$	$\frac{x}{c}$
0	1.0000	0	0	0	1.000	0	0
.005	.9900	.1411	.1415	$\frac{\pi}{20}$	.9877	.1684	.0062
.0075	.9850	.1725	.1734	$\frac{\pi}{10}$	.9511	.3090	.0214
.0125	.9750	.2222	.2241	$\frac{3\pi}{20}$	.9010	.4540	.0545
.025	.9500	.3122	.3176	$\frac{3\pi}{10}$	.8000	.5678	.0955
.05	.9000	.4359	.4510	$\frac{5\pi}{20}$	.7071	.7071	.1465
.075	.8500	.5268	.5548	$\frac{3\pi}{10}$	.5678	.8090	.2061
.10	.8000	.6000	.6435	$\frac{7\pi}{20}$	.4540	.8910	.2730
.15	.7000	.7141	.7954	$\frac{4\pi}{10}$	.3090	.9511	.3455
.20	.6000	.8000	.9273	$\frac{9\pi}{20}$	.1564	.9877	.4218
.25	.5000	.8660	1.0472	$\frac{5\pi}{10}$	0	1.0000	.5000
.30	.4000	.9165	1.1593	$\frac{11\pi}{20}$	-.1564	.9877	.5782
.35	.3000	.9539	1.2661	$\frac{6\pi}{10}$	-.3090	.9511	.6545
.40	.2000	.9798	1.3694	$\frac{13\pi}{20}$	-.4540	.8910	.7270
.45	.1000	.9950	1.4706	$\frac{7\pi}{10}$	-.5678	.8090	.7939
.50	0	1.000	1.5708	$\frac{15\pi}{20}$	-.7071	.7071	.8536
.55	-.1000	.9950	1.6710	$\frac{8\pi}{10}$	-.8090	.5678	.9045
.60	-.2000	.9798	1.7722	$\frac{17\pi}{20}$	-.8910	.4540	.9455
.65	-.3000	.9539	1.8755	$\frac{9\pi}{10}$	-.9511	.3090	.9755
.70	-.4000	.9165	1.9823	$\frac{19\pi}{20}$	-.9877	.1564	.9939
.75	-.5000	.8660	2.0944	$\pi$	-1.000	0	1.0000
.80	-.6000	.8000	2.2143				
.85	-.7000	.7141	2.3462				
.90	-.8000	.6000	2.4981				
.95	-.9000	.4359	2.6906				
1.0	-1.0000	0	3.1416				

TABLE VI.—INTEGRATION CALCULATION OF  $\circ P_b$  FOR NACA 4412 MEAN CAMBER LINE

$\theta$	$\cos \theta$	$\sin \theta$	$\frac{dy_c}{dx}$	$\frac{d}{d\theta} \left( \frac{dy_c}{dx} \right)$	$\frac{\circ P_b}{4}$	$\circ P_b$	$x/c$
0	1.0000	0	0.2000	0	0	0	0
$\pi/10$	.9511	.3090	.1578	-.0773	-.0635	.334	.0244
$2\pi/10$	.8090	.5678	.1623	-.1470	-.1279	.812	.0955
$3\pi/10$	.5678	.8090	.0870	-.2023	-.1705	.683	.2061
$4\pi/10$	.3090	.9511	-.0278	-.2378	-.1823	.729	.3455
$5\pi/10$	0	1.0000	-.0222	-.1111	-.1668	.627	.5000
$6\pi/10$	-.3090	.9511	-.0366	-.1056	-.1367	.547	.6545
$7\pi/10$	-.5678	.8090	-.0575	-.0899	-.1114	.446	.7939
$8\pi/10$	-.8090	.5678	-.1121	-.0633	-.0793	.319	.9045
$9\pi/10$	-.9511	.3090	-.1279	-.0343	-.0412	.162	.9755
$\pi$	-1.0000	0	-.1333	0	0	0	1.0000
$11\pi/10$			-.1279				
$12\pi/10$			-.1121				
$13\pi/10$			-.0875				
$14\pi/10$			-.0566				
$15\pi/10$			-.0222				
$16\pi/10$			.0273				
$17\pi/10$			.0870				
$18\pi/10$			.1623				
$19\pi/10$			.1578				
$2\pi$			-.2000				

TABLE VII.—MEAN-CAMBER-LINE LIFT DISTRIBUTION CALCULATION FOR NACA 4412 AIRFOIL SECTION

$x/c$	$\frac{\circ P_a}{c l_a}$	$\circ P_b$	$\frac{V_f}{V_\infty}$	$P_a (c l_a = 1)$	$\frac{P_a}{c l_a}$	$P_b$
0	$\infty$	0	0	0	0	0
.0125	5.658	.275	0.987	5.580	5.408	.271
.0250	3.976	.328	1.099	4.371	4.235	.355
.0500	2.775	.406	1.163	3.229	3.126	.472
.0750	2.236	.469	1.181	2.641	2.560	.554
.1000	1.910	.522	1.188	2.289	2.199	.620
.1500	1.515	.610	1.187	1.799	1.742	.724
.2000	1.273	.671	1.179	1.500	1.454	.792
.2500	1.103	.708	1.168	1.288	1.248	.828
.3000	.973	.727	1.156	1.125	1.090	.841
.4000	.780	.710	1.129	.831	.854	.802
.5000	.637	.629	1.103	.702	.681	.694
.6000	.520	.577	1.078	.569	.542	.622
.7000	.417	.517	1.050	.437	.424	.543
.8000	.318	.441	1.022	.325	.315	.451
.9000	.212	.326	.982	.208	.202	.320
.9500	.146	.241	.942	.138	.134	.227
1.0000	0	0		0	0	0
				$c l_a (c l_a = 1)$ = 1.032		$c l_b = 0.587$

TABLE VIII.—VELOCITY DISTRIBUTION CALCULATION FOR NACA 4412 AIRFOIL SECTION AT  $c_l = 0.72$

$x/c$	$P_b$ ( $c l_b = 0.587$ )	$\frac{P_a}{c l_a}$ ( $c l_a = c l_b$ )	$P$ ( $c l = 0.72$ )	$\frac{V_f}{V_\infty}$	$\frac{P}{\frac{4}{V_f}}$	$\frac{V_a}{V_\infty}$	$\frac{V_1}{V_\infty}$
0	0	0	0	0			
.0125	.271	.719	.990	.987	0.251	1.238	0.736
.0250	.355	.683	.918	1.099	.209	1.308	.890
.0500	.472	.415	.887	1.163	.191	1.354	.972
.0750	.554	.340	.894	1.181	.189	1.372	.994
.1000	.620	.292	.912	1.188	.192	1.382	.998
.1500	.724	.232	.956	1.187	.201	1.388	.986
.2000	.792	.198	.985	1.179	.209	1.388	.970
.2500	.828	.166	.994	1.168	.213	1.381	.953
.3000	.841	.145	.956	1.156	.213	1.369	.943
.4000	.802	.114	.916	1.129	.208	1.332	.926
.5000	.694	.091	.785	1.103	.178	1.281	.925
.6000	.622	.071	.668	1.076	.161	1.237	.915
.7000	.543	.056	.599	1.050	.143	1.193	.907
.8000	.451	.042	.498	1.022	.120	1.142	.902
.9000	.320	.027	.347	.982	.088	1.070	.894
.9500	.227	.018	.245	.942	.065	1.007	.877
1.0000	0	0	0				

TABLE IX—SURFACE ORDINATES AND VELOCITIES FOR ELLIPTIC BASE PROFILES

y/c	t/c=0.02		t/c=0.04		t/c=0.06		t/c=0.08		t/c=0.10		t/c=0.12		t/c=0.14		
	y/c	V <sub>r</sub> /V <sub>∞</sub>	y/c	V <sub>r</sub> /V <sub>∞</sub>											
0	0	0	0	0	0	0	0	0	0	0	0	0	0	0	
.005	.001411	1.0099	.002821	1.0013	.004232	1.9789	.005643	1.9417	.007053	1.9003	.008464	1.8567	.009875	1.8132	
.0075	.001728	1.0134	.003451	1.0139	.005177	1.0028	.006902	1.9824	.008628	1.9553	.010353	1.9240	.012079	1.8906	
.0125	.002222	1.0162	.004444	1.0244	.006666	1.0251	.008888	1.0190	.011110	1.0073	.013332	1.9910	.015554	1.9714	
.025	.003123	1.0182	.006245	1.0324	.009368	1.0428	.012490	1.0494	.015613	1.0524	.018735	1.0521	.021858	1.0488	
.050	.004359	1.0191	.008718	1.0365	.013077	1.0520	.017436	1.0656	.021795	1.0773	.026153	1.0871	.030512	1.0952	
.075	.005288	1.0194	.010536	1.0378	.015803	1.0551	.021071	1.0711	.026339	1.0859	.031607	1.0996	.036875	1.1120	
.100	.006000	1.0196	.012000	1.0385	.018000	1.0566	.024000	1.0740	.030000	1.0904	.036000	1.1059	.042000	1.1206	
.150	.007141	1.0198	.014283	1.0392	.021424	1.0582	.028568	1.0767	.035707	1.0948	.042849	1.1123	.049690	1.1294	
.200	.008000	1.0199	.016000	1.0395	.024000	1.0589	.032000	1.0781	.040000	1.0909	.048000	1.1155	.056000	1.1338	
.250	.008600	1.0199	.017321	1.0397	.025981	1.0594	.034641	1.0788	.043301	1.0962	.051962	1.1173	.060822	1.1303	
.300	.009165	1.0199	.018330	1.0398	.027495	1.0596	.036661	1.0793	.045826	1.0989	.054991	1.1185	.064166	1.1379	
.350	.009539	1.0200	.019079	1.0399	.028618	1.0598	.038168	1.0797	.047697	1.0995	.057236	1.1192	.066776	1.1389	
.400	.009798	1.0200	.019696	1.0400	.029394	1.0599	.039192	1.0799	.048990	1.0998	.058788	1.1197	.068486	1.1395	
.450	.009950	1.0200	.019900	1.0400	.029850	1.0600	.039800	1.0800	.049749	1.0999	.059099	1.1199	.069049	1.1399	
.500	.010000	1.0200	.020000	1.0400	.030000	1.0600	.040000	1.0800	.050000	1.1000	.060000	1.1200	.070000	1.1400	
.550	.009950	1.0200	.019900	1.0400	.029850	1.0600	.039800	1.0800	.049749	1.0999	.059099	1.1199	.069049	1.1399	
.600	.009798	1.0200	.019696	1.0400	.029394	1.0599	.039192	1.0799	.048990	1.0998	.058788	1.1197	.068486	1.1395	
.650	.009539	1.0200	.019079	1.0399	.028618	1.0598	.038168	1.0797	.047697	1.0995	.057236	1.1192	.066776	1.1389	
.700	.009165	1.0199	.018330	1.0398	.027495	1.0596	.036661	1.0793	.045826	1.0989	.054991	1.1185	.064166	1.1379	
.750	.008600	1.0199	.017321	1.0397	.025981	1.0594	.034641	1.0788	.043301	1.0962	.051962	1.1173	.060822	1.1303	
.800	.008000	1.0199	.016000	1.0395	.024000	1.0589	.032000	1.0781	.040000	1.0909	.048000	1.1155	.056000	1.1338	
.850	.007141	1.0198	.014283	1.0392	.021424	1.0582	.028568	1.0767	.035707	1.0948	.042849	1.1123	.049690	1.1294	
.900	.006000	1.0196	.012000	1.0385	.018000	1.0566	.024000	1.0740	.030000	1.0904	.036000	1.1059	.042000	1.1206	
.950	.004359	1.0191	.008718	1.0365	.013077	1.0520	.017436	1.0656	.021795	1.0773	.026153	1.0871	.030512	1.0952	
1.000	0	0	0	0	0	0	0	0	0	0	0	0	0	0	
$\frac{TL.E.}{c} - \frac{TT.E.}{c} = 0.00020$		$\frac{TL.E.}{c} - \frac{TT.E.}{c} = 0.00080$		$\frac{TL.E.}{c} - \frac{TT.E.}{c} = 0.01180$		$\frac{TL.E.}{c} - \frac{TT.E.}{c} = 0.00320$		$\frac{TL.E.}{c} - \frac{TT.E.}{c} = 0.00500$		$\frac{TL.E.}{c} - \frac{TT.E.}{c} = 0.00720$		$\frac{TL.E.}{c} - \frac{TT.E.}{c} = 0.00950$			

TABLE X.—BASE PROFILE ORDINATE CALCULATION FOR SEMI-LOW-DRAG AIRFOIL

x/c	(V <sub>r</sub> /V <sub>∞</sub> ) <sub>1</sub>	V <sub>r</sub> /V <sub>∞</sub>	(Δv/V <sub>∞</sub> ) <sub>1</sub>	Cos θ	( $\frac{\Delta v}{V_{\infty}}$ ) <sub>1</sub>	θ (radians)	(Δv/V <sub>∞</sub> ) <sub>2</sub>	( $\frac{\Delta v}{V_{\infty}}$ ) <sub>2</sub>	Δ(Δv/V <sub>∞</sub> )	Δv/V <sub>∞</sub>	V <sub>r</sub> /V <sub>∞</sub>	Δy/c	y/c	y/c
0	0	0	0	1.000	0	0	0	0	0.0020	(.0020)	0	0	0	0
.0125	.064	1.0026	-.039	.975	-.038	.2241	-.0390	-.0380	.0019	-.0371	0.9655	0	.02007	.02007
.0250	.1082	1.1228	-.041	.950	-.039	3.176	-.0410	-.0390	.0018	-.0382	1.0834	.00004	.02796	.02796
.0500	.1150	1.1948	-.036	.930	-.032	4.510	-.0359	-.0323	.0018	-.0341	1.1605	.00027	.03795	.03822
.0750	.1185	1.2151	-.030	.850	-.026	5.548	-.0304	-.0268	.0017	-.0287	1.1864	.00084	.04470	.04554
.1000	.1196	1.2206	-.025	.800	-.020	6.435	-.0248	-.0198	.0017	-.0231	1.1975	.00161	.04959	.05120
.1500	.1201	1.2154	-.014	.700	-.010	7.954	-.0137	-.0096	.0016	-.0121	1.2033	.00383	.05587	.05940
.2000	.1199	1.2019	-.008	.600	-.002	9.273	-.0027	-.0016	.0015	-.0012	1.2007	.00872	.05902	.06474
.3000	.1188	1.1668	.000	.400	.008	1.1693	.0191	.0076	.0014	.0205	1.1873	.01032	.05036	.05938
.4000	.1169	1.1284	.041	.200	.008	1.3694	.0410	.0082	.0012	.0422	1.1706	.01439	.05462	.06291
.5000	.1151	1.0896	.081	0	0	1.5708	.0810	0	.0011	.0621	1.1517	.01634	.04649	.06283
.6000	.1098	1.0511	.045	-.200	-.009	1.7722	.0440	-.0088	.0010	.0450	1.0961	.01491	.03649	.05140
.7000	.1041	1.0135	.027	-.400	-.011	1.9323	.0245	-.0098	.0008	.0253	1.0393	.01132	.02562	.03694
.8000	.936	.9789	.009	-.800	-.005	2.1443	.0047	-.0028	.0007	.0084	.9823	.00621	.01491	.02182
.9000	.932	.9416	-.010	-.800	.008	2.4961	-.0154	.0123	.0005	-.0149	.9267	.00271	.00559	.00830
.9500	.905	.9243	-.019	-.900	.017	2.6906	-.0260	.0234	.0004	-.0256	.8937	.00100	.00203	.00303
1.0000	.879	.8072	-.028	-1.000	.023	3.1416	-.0380	.0380	.0002	-.0378	.8694	0	0	0

TABLE XI.—INTEGRATION CALCULATION OF  $\frac{d(\Delta y_1)}{dx}$  FOR BASE PROFILE OF SEMI-LOW-DRAG AIRFOIL

θ	$\frac{\Delta v}{V_{\infty}}$	$\frac{d}{d\theta} (\frac{\Delta v}{V_{\infty}})$	$\frac{d(\Delta y_1)}{dx}$	$\frac{x}{c}$
0	0	0	0	0
π/10	-.0391	.0224	.00564	.0244
2π/10	-.0244	.0650	.03358	.0955
3π/10	.0001	.0889	.04589	.2061
4π/10	.0305	1.019	.04225	.3455
5π/10	.0621	0	.00266	.6000
6π/10	.0845	-.0214	-.03721	.6545
7π/10	.0066	-.0843	-.04441	.7989
8π/10	-.0158	-.0826	-.03720	.9045
9π/10	-.0314	-.0364	-.02164	.9758
π	-.0378	0	0	1.0000
11π/10	-.0314	-----	-----	-----
12π/10	-.0158	-----	-----	-----
13π/10	.0066	-----	-----	-----
14π/10	.0845	-----	-----	-----
15π/10	.0621	-----	-----	-----
16π/10	.0305	-----	-----	-----
17π/10	.0001	-----	-----	-----
18π/10	-.0244	-----	-----	-----
19π/10	-.0391	-----	-----	-----
2π	0	-----	-----	-----

TABLE XII.—MEAN-CAMBER-LINE-ORDINATE CALCULATION FOR SEMI-LOW-DRAG AIRFOIL

$x/c$	$V_{\infty}/V_0$	$V_1/V_0$	$\alpha P_1$	$\frac{\alpha P_1}{4}$	$\theta$	$V_1/V_0$	$P_1$	$\frac{V_1}{c}$	$\frac{dy_1}{dx}$	$\frac{y_1}{c}$	$\frac{dy_1}{dx}$
0	0	0	0	0	0	0	0	0	0.0632	0	0.0765
.0125	.9697	.9412	.0970	.02425	.2241	.9665	.0937	.00085	.0702	.00100	.0825
.0250	1.1296	1.0371	.1850	.04625	.3176	1.0824	.2004	.00173	.0712	.00204	.0869
.0500	1.2242	1.0968	.2648	.09370	.4510	1.1605	.2957	.00341	.0592	.00403	.0715
.0750	1.2579	1.1149	.2860	.07150	.5543	1.1894	.3598	.00454	.0320	.00466	.0448
.1000	1.2708	1.1243	.2930	.07325	.6455	1.1975	.3709	.00506	.0118	.00630	.0226
.1500	1.2710	1.1355	.2710	.06775	.7854	1.2083	.3261	.00494	.0148	.00679	.0025
.2000	1.2594	1.1421	.2346	.05865	.9273	1.2007	.2817	.00372	.0390	.00618	.0207
.3000	1.2202	1.1544	.1816	.03220	1.1593	1.1873	.1862	.00062	.0356	.00265	.0438
.4000	1.1719	1.1894	.0050	.00125	1.3694	1.1706	.0069	.00669	.0563	.00176	.0440
.5000	1.1211	1.1823	-.1224	-.03080	1.5708	1.1517	-.1410	.00122	.0325	.00506	.0202
.6000	1.0716	1.1206	-.0850	-.02450	1.7722	1.0361	-.1074	.00126	.0108	.00356	.0017
.7000	1.0204	1.0572	-.0736	-.01840	1.9323	1.0858	-.0765	.00137	0	.00308	.0123
.8000	.9701	.9946	-.0490	-.01220	2.1435	.9523	-.0481	.001347	.0044	.00360	.0107
.9000	.9205	.9328	-.0246	-.00616	2.4881	.9267	-.0225	.001291	.0064	.00181	.0187
.9500	.8957	.9018	-.0122	-.00308	2.6806	.8987	-.0110	.001259	.0061	.00058	.0184
1.0000	.8694	.8694	0	0	3.1416	.8694	0	.001233	.0037	0	.0160

TABLE XIII.—INTEGRATION CALCULATION FOR MEAN CAMBER LINE OF SEMI-LOW-DRAG AIRFOIL

$\theta$	$\frac{\alpha P}{4}$	$\frac{d}{dx} (\frac{\alpha P}{4})$	$\frac{dy_1}{dx}$	$x/c$
0	0	0	0.06320	0
$\pi/10$	-.0456	.2120	.07120	.0244
$2\pi/10$	-.0734	0	.01363	.0955
$3\pi/10$	-.0875	-.0934	-.03469	.2061
$4\pi/10$	-.0189	-.1542	-.06026	.3455
$5\pi/10$	-.0806	-.0185	-.02263	.5000
$6\pi/10$	-.0212	.0293	-.00873	.6545
$7\pi/10$	-.0126	.0248	.00429	.7939
$8\pi/10$	-.0059	.0175	.00624	.9045
$9\pi/10$	-.0010	.0098	.00520	.9756
$\pi$	0	0	.00368	1.0000
$11\pi/10$	.0015	-----	-----	-----
$12\pi/10$	.0059	-----	-----	-----
$13\pi/10$	.0126	-----	-----	-----
$14\pi/10$	.0212	-----	-----	-----
$15\pi/10$	.0306	-----	-----	-----
$16\pi/10$	.0189	-----	-----	-----
$17\pi/10$	-.0575	-----	-----	-----
$18\pi/10$	-.0734	-----	-----	-----
$19\pi/10$	-.0455	-----	-----	-----
$2\pi$	0	-----	-----	-----

TABLE XIV.—CALCULATION OF ORDINATES OF SEMI-LOW-DRAG AIRFOIL

$x/c$	$\frac{y_1}{c}$	$\frac{y_1}{c} \sin \theta$	$\frac{y_1}{c} \cos \theta$	$\frac{y_2}{c}$	$\frac{x_2}{c}$	$\frac{y_2}{c}$	$\frac{x_1}{c}$	$\frac{y_1}{c}$
0	0	0	0	0	0	0	0	0
.0125	.02007	.00165	.02000	.00100	.01095	.02100	.01415	.01900
.025	.02790	.00282	.02780	.00204	.02268	.02964	.02732	.02576
.05	.03822	.00473	.03812	.00403	.04727	.04216	.05273	.03409
.075	.04554	.00702	.04549	.00546	.07288	.05065	.07702	.04003
.1	.05120	.00912	.05118	.00679	.08679	.06748	.10121	.04488
.15	.05940	.01015	.05940	.00679	.15015	.06810	.14985	.05281
.2	.06474	.01134	.06473	.00618	.20134	.07091	.18366	.05855
.3	.06968	.01202	.06962	.00258	.30302	.07250	.29698	.06674
.4	.06891	.01303	.06884	.00176	.40303	.06708	.39697	.07090
.5	.06283	.01127	.06282	.00506	.50127	.05776	.49873	.06788
.6	.05140	.00909	.05140	.00586	.59991	.04584	.60009	.05726
.7	.03694	.00645	.03694	.00508	.69956	.03186	.70045	.04202
.8	.02182	.00336	.02182	.00360	.79861	.01822	.80036	.02542
.9	.00830	.00016	.00830	.00181	.89884	.00640	.90016	.01011
.95	.00303	.00008	.00303	.00088	.94994	.00215	.95006	.00391
L 0	0	0	0	0	1.00000	0	1.00000	0

TABLE XV.—ORDINATES AND VELOCITY DISTRIBUTIONS FOR "DOUBLE-ROOF" BASE PROFILES

$x/c$	$\frac{x_2}{c} = 0.2$		$\frac{x_2}{c} = 0.3$		$\frac{x_2}{c} = 0.4$		$\frac{x_2}{c} = 0.5$		$\frac{x_2}{c} = 0.6$		$\frac{x_2}{c} = 0.7$		$\frac{x_2}{c} = 0.8$		$\frac{x_2}{c} = 0.9$	
	$\frac{\Delta y}{sc}$	$\frac{\Delta y}{sV_0}$														
0	0	0	0	0	0	0	0	0	0	0	0	0	0	0	0	0
.0125	.000435	-.104984	.000503	-.136122	.000551	-.161039	.000588	-.181690	.000618	-.199224	.000642	-.0.214352	.000662	-.0.227671	.000680	-.0.239465
.025	.001210	-.092485	.001404	-.111122	.001542	-.148339	.001648	-.169190	.001732	-.187224	.001801	-.201882	.001859	-.215171	.001909	-.226453
.05	.003301	-.054984	.003869	-.086122	.004271	-.111039	.004576	-.131690	.004818	-.149224	.005017	-.164382	.005184	-.177671	.005326	-.189486
.075	.005829	-.029985	.006914	-.061122	.007672	-.086039	.008248	-.106890	.008701	-.124224	.009073	-.139382	.009384	-.152671	.009645	-.164465
.10	.008593	-.004984	.010336	-.036122	.011540	-.061039	.012445	-.081690	.013159	-.099224	.013742	-.114382	.014226	-.127671	.014648	-.139456
.15	.014240	.045016	.017788	.013878	.020156	.011039	.021899	-.081690	.023279	-.049224	.024338	-.064382	.025318	-.077671	.026104	-.085455
.20	.019003	.095016	.025375	.063878	.029348	.038961	.032189	-.018310	.034407	.000776	.036194	-.014382	.037671	-.027671	.038610	-.039455
.25	.021278	.067515	.032318	.118878	.038427	.068961	.042716	.068810	.048990	.050776	.048805	.035618	.050753	.022329	.052578	-.010546
.30	.022122	.078414	.037549	.168878	.046854	.138961	.052985	.118310	.057561	.100776	.061181	.085618	.064111	.072229	.068822	.060546
.35	.022087	.070113	.039419	.147005	.068940	.188961	.062492	.168310	.068889	.150776	.073517	.135618	.077433	.122329	.050697	.110546
.40	.021421	.061812	.039267	.130132	.068333	.238961	.060673	.218310	.078920	.200776	.085216	.185618	.090267	.172329	.094446	.160546
.45	.020277	.053512	.037318	.118269	.068791	.209149	.076597	.268310	.067780	.250776	.095644	.235618	.102268	.222329	.107521	.150546
.50	.018766	.045211	.035433	.096356	.066405	.179336	.079377	.218310	.065810	.240776	.104997	.265618	.113040	.272329	.119560	.160546
.55	.018978	.036910	.032351	.076512	.052327	.149524	.076797	.268310	.068080	.230776	.112667	.335618	.122137	.322329	.130171	.150546
.60	.014966	.028609	.028767	.062639	.047056	.119712	.070673	.218310	.098170	.200776	.116358	.385618	.129026	.372329	.128907	.160546
.65	.012856	.020309	.024940	.046786	.040466	.089900	.062492	.168310	.090466	.136181	.116810	.435618	.133044	.422329	.145229	.140546
.70	.010648	.012008	.020646	.028893	.034974	.060087	.052986	.118310	.078590	.233060	.111269	.485618	.138263	.472329	.148456	.160546
.75	.008427	.003707	.016402	.012020	.027421	.030275	.042716	.068310	.064448	.149202	.095767	.337464	.128169	.822329	.147729	.150546
.80	.006254	-.004594	.012214	-.004953	.020520	.000463	.032189	.018310	.078590	.065844	.075192	.189289	.114466	.872329	.141606	.160546
.85	.004203	-.012895	.008232	-.021727	.013880	-.029850	.021892	-.031690	.038503	-.018514	.052712	.041124	.068773	.271152	.127612	.150546
.90	.002382	-.021196	.004637	-.035600	.007344	-.059162	.012445	-.081690	.019354	-.102373	.030626	-.107040	.051762	-.030024	.090662	.160546
.925	.001588	-.025346	.003061	-.047036	.005186	-.074068	.008248	-.106890	.012868	-.144202	.020458	-.181122	.085114	-.180618	.073464	.205183
.95	.000861	-.029496	.001693	-.055473	.002573	-.088974	.004576	-.131690	.007163	-.188231	.011466	-.255205	.019886	-.311201	.043071	.250179
.975	.000309	-.033647	.000608	-.068909	.001033	-.103850	.001648	-.156890	.002687	-.228160	.004161	-.329287	.007291	-.481739	.016366	.205541
.9875	.000110	-.038722	.000217	-.081128	.000363	-.111333	.000888	-.169190	.000924	-.249124	.001490	-.368328	.002622	-.557083	.008974	.208222
1.000	0	-.037797	0	-.072346	0	-.118757	0	-.181690	0	-.270089	0	-.403369	0	-.632377	0	-.1.160004